UNIVERSITY OF CALIFORNIA
RIVERSIDE

Pathophysiology of Juvenile Traumatic Brain Injury: Role of Edema and a Potential Treatment

A Dissertation submitted in partial satisfaction
of the requirements for the degree of

Doctor of Philosophy

in

Neuroscience

by

Arash Matthew Adami

August 2013

Dissertation Committee:
Dr. Andre Obenaus, Co-Chairperson
Dr. Margarita Curras-Collazo, Co-Chairperson
Dr. Michael Adams

The Dissertation of Arash Matthew Adami is approved:

_____

_____

Committee Co-Chairperson

_____

Committee Co-Chairperson

University of California, Riverside

Acknowledgements

First, I would like to thank my wife. Without her, I would have gone insane. She endured many years of late nights and long weekends in the lab and was my driving force to finish. She stuck with me the entire way. I would like to thank my parents, sister, in-laws, extended family, and close friends. Their love, support, and words of encouragement helped me overcome every obstacle.

This dissertation would not be possible without the support from UC Riverside faculty and staff. I want to give special thanks to my graduate advisor, Dr. André Obenaus, who pushed me to continually improve my scientific technique. He taught me one simple truth which I will carry with me throughout my career: trust but verify. I would also like to thank my dissertation committee, Dr. Michael Adams and Dr. Margarita Curras-Collazo. Dr. Adams served as the department chair most of my years in graduate school and, despite a busy schedule, was always willing to listen. Lastly, I wanted to thank Dr. Margarita Curras-Collazo, who was my inspiration in pursuing a career in neuroscience. After taking her undergraduate class, Systems Neuroscience, I was hooked. She graciously accepted me into her lab as an assistant and she became a trusted mentor for 8 years. She referred me to Dr. Obenaus to further my post-undergraduate career and, if not for her, I would never have discovered my passion for magnetic resonance imaging and traumatic brain injury. She may not

know this, but if she did not refer me to Dr. Obenaus's lab in the summer of 2007, I would have never met my wife!

Other faculty members from whom I have learned include Dr. Currie, Dr. Razak, Dr. Hickmott, Dr. Fiacco, Dr. Korzus, Dr. Stanley, and Drs. Ethell. From their one on one conversations, exemplary teaching style, or compassionate critique of my research, these individuals have pushed me to think critically. Also, I cannot forget to mention the staff that supports the graduate students, especially Perla Fabelo. Her positive attitude and continually supportive presence was priceless.

At Loma Linda University, there are several individuals who helped me problem solve specific issues or steered me in the right direction, ultimately forming me into the scientist I am today. First, Dr. Jerome Badaut was gracious enough to let me work on his NIH grant, which later became the foundation of my dissertation. His strong analytical skills and goal-oriented vision sets him apart as a superior scientist. Dr. Ashwal, the clinician guru, always surprised me by responding with a fully edited document in two hours, no matter what size I had sent for review. When I wanted to discuss complex MRI sequencing issues or needed career advice, Dr. Shu-Wei Sun was always available to talk. Long conversations in the break room or attending group outings, including rock climbing, with Dr. Samuel Barnes, Dr. Roman Vlkolinsky, and Dr. Lei Huang helped me forget the hardships of graduate school and provided a sense of community.

I will never forget the unwavering devotion from Sonny Kim, Beatriz Tone, Kamal Ambadipudi, Pete Hayes, Mary Hamer, Dr. Christine Turenius-Bell, Anna Smith, and Dr. Viorela Pop. A special thanks to Beatriz and Sonny, who taught me professionalism in the workplace and lessons that have already helped guide me in my career. They were my mother and father figures in the lab, listening to me when I was frustrated, searching for things that I could not find, and just helping the lab run smoothly.

Lastly, I would like to give special recognition to the “slackers” who did all the work in the lab. One way or another, Dr. Julia Evans, Jacqueline Coats, Virginia Donovan, Elyse Kite, Emil Rudobeck, David Ajao, and Andrew Fukuda had their hand in my dissertation. Then, there were the fellow graduate students that participated in the venting ritual at Getaway Cafe: Zev Wisotsky, Charles Abbott III, Fred Lawton, Jenni Deveau, Hani El Shawa, Clement David, and Matt Valdez. A special thanks to Eric McCoy and Patrick Davis, the greatest friends and 5AM gym partners for whom a graduate student could have ever asked.

Some people think my acknowledgements on my manuscripts, posters, and presentations are too long and this diminishes the significance of the important few. But to me, I truly believe that each one of these people contributed to the success of my Ph.D. during these past 5 years. Every conversation, time spent away from their work, and time away from their friends and family to help me deserves recognition.

Chapter 3 of this dissertation, in part, is a reprint of the material as it appears in Badaut, Ashwal, Adami, Tone, Recker, Spagnoli, Ternon, and Obenaus, JCBFM, 2011 Mar; 31(3):819-31. Chapter 4 of this dissertation, in part, is a reprint of the material as it appears in Fukuda, Adami, Pop, Bellone, Coats, Hartman, Ashwal, Obenaus, and Badaut, JCBFM, 2013; doi: 10.1038.

ABSTRACT OF THE DISSERTATION

Pathophysiology of Juvenile Traumatic Brain Injury:
Role of Edema and a Potential Treatment

by

Arash Matthew Adami

Doctor of Philosophy, Graduate Program in Neuroscience
University of California, Riverside, August 2013
Dr. Andre Obenaus, Co-Chairperson
Dr. Margarita Curras-Collazo, Co-Chairperson

Traumatic brain injury (TBI) is caused by an external force to the head, resulting in damage to the brain. TBI is especially common in children and young adults and is associated with long-term mortality and morbidity. Juveniles seem to be at increased risk of developing cerebral edema after TBI partly due to higher water content and developmental differences in the brain's response to injury. Aquaporin-4 (AQP4) is the most abundant water channel in the brain and plays a critical role in edema formation. Edema formation can be attributed to cellular swelling (cytotoxic edema) or breakdown of the blood-brain barrier (BBB). This dissertation examined the lesion composition (percentage of blood and edema) after graded juvenile TBI (jTBI) and role of AQP4 in the normal and pathologic rodent brain. Using an established rodent model of focal jTBI, we characterized the composition of the lesion using magnetic resonance imaging (MRI). We found that 1 day after jTBI, the lesion was ~60% edema and ~40% blood. At 3 days, the edema volume decreased in all severity groups and the

extravascular blood volume in the lesion remained unchanged. To understand water mobility in the brain after jTBI, we first evaluated the effects of knocking down AQP4 using RNA interference in an uninjured juvenile rodent brain. We demonstrated that a 27% decrease in AQP4 protein expression, induced by small interfering RNA against AQP4 (siAQP4), lead to a 50% reduction in water mobility using MRI. We then investigated the effect of siAQP4 injection in a juvenile rodent brain after TBI. We identified improved neurologic testing and physiologic measures, including reduced edema formation, neuronal cell death, astrogliosis, and BBB, in rat pups treated with siAQP4. Given these results, knockdown of AQP4 may prove to be an effective therapy in the early time course after jTBI.

Table of Contents

List of Figures

Chapter 1

General Introduction

Pediatric Traumatic Brain Injury

Traumatic brain injury (TBI) is the result of an external force to the head effecting damage either from penetration of the skull or from rapid brain acceleration or deceleration (Bullinger et al., 2002). TBI is a major public health problem, especially among young children under 5 years, adolescents between 15-25 years, and the elderly over 75 years (Jennett, 1998). Juvenile TBI (jTBI), also referred to as pediatric TBI, has recently gained attention among clinicians as data has indicated that hospital admission rates for head injuries resulted in half a million emergency department visits for TBI; this number continues to rise (Faul M, 2010). Epidemiological data has demonstrated the serious socioeconomic impact of TBI among children. It is estimated that the cost of hospital care alone for jTBI exceeds $1 billion per year (Kraus et al., 1990). An estimated 170,000 children who survive TBI in the United States each year suffer from diffuse and widespread injury, resulting in motor and cognitive impairments. The neuropathological sequelae that result from TBI include a complex cascade of events – namely edema formation and brain swelling which contribute to secondary ischemic injuries. Children are especially vulnerable to the development of cerebral edema. Experimental studies using young rats

demonstrated that this may be partly due to higher brain water content in young rats (Dobbing and Sands, 1981), to increased inflammatory response in the immature brain (Clark et al., 1996), or to structural differences in the developing brain versus the adult (Ciurea et al., 2011). Despite the commonly held view that developing brains are able to adapt to the impact of severe insults, clinical reports have residual deficits over a range of skills, including intellectual ability, attention, and memory (Taylor and Alden, 1997, Fulton et al., 2012). These deficits potentially interfere with development, thereby reducing the child's ability to acquire knowledge and skills and causing gaps between the abilities of injured children and those of their peers.

The most common form of brain injury is mild TBI, which occurs despite lack of external injuries, loss of consciousness, or microstructural lesions in the white matter (Inglese et al., 2005, Suh et al., 2006, Anderson-Barnes et al., 2010). It is estimated that at least 75% of all TBI in the US are mild in severity; this number is likely much larger given a lack of data on individuals who do not seek medical attention. Recently, publicized sports-related TBI and media focus on military injuries in the adult literature have stimulated interest in the consequences at younger ages (Anderson-Barnes et al., 2010). A more unfortunate event is moderate to severe TBI resulting in long-term or permanent disability. The Glasgow Coma Scale is the gold standard for head injury severity scoring clinically (Gotschall et al., 1995). Using size and location of lesion and using magnetic resonance imaging (MRI) can improve the ability of measuring

severity of TBI. The numbers of affected individuals, the costs necessary to facilitate their care and rehabilitation coupled with the lack of therapies indicate that TBI requires urgent research attention for better understanding of the trauma pathophysiology and its treatment.

Roles of Edema

TBI is divided into primary injuries, the result of a direct and immediate biomechanical disruption of the brain tissue, and secondary injuries, a matrix of several delayed events affecting brain tissue. Thus, development of efficient post-injury therapeutic treatments should focus on targeting the secondary injury cascades (Morales et al., 2005). This is especially important in jTBI because the brain is still in its developmental stages and secondary injuries are more severe in the pediatric population with long lasting effects in the child's cognitive, emotional, and motor functions (Moran et al., 2012). Secondary injuries, including blood-brain barrier (BBB) disruption and edema formation, are pathological hallmarks after jTBI and responsible for the multitude of long lasting consequences (Margulies and Hicks, 2009), and make excellent clinical targets for improving recovery.

Brain volume and cerebral homeostasis rely heavily on the functional integrity of the BBB. Structural or functional impairment of the BBB after TBI leads to vasogenic edema. The BBB contain cerebral endothelial cells that are sealed together by tight junctions, thus preventing uncontrolled passage of

proteins (Reese and Karnovsky, 1967). Vasogenic brain edema is characterized by a protein-rich exudate derived from plasma resulting from an increased permeability of the capillary endothelial cells to albumin and other plasma proteins (Betz et al., 1989).

Cytotoxic edema is characterized as sustained water accumulation in the cell. This occurs independently of BBB integrity, as opposed to vasogenic edema. Under physiological conditions, the sodium potassium pump allows for the influx of osmotically active solutes such as Na^+, which is balanced by their active, energy-dependent elimination. This process prevents a consecutive influx of water and cellular swelling. Following TBI, increased uptake of Na^+ causes a shift in the pump equilibrium, which cannot be counteracted by the active sodium potassium pump. As energy depletion continues during cerebral ischemia related to structural and functional mitochondrial impairment, sodium potassium pump failure and aggravates cytotoxic brain edema proliferates (Unterberg et al., 2004).

AQP4 and its Role in the Brain

The discovery of specific brain aquaporins (AQPs, water channels) suggested new approaches to more accurately investigate water movement within the central nervous system. Aquaporin-4 (AQP4) is mainly expressed in perivascular astrocytic endfeet and is the most abundant aquaporin in the brain and has been hypothesized to play a central role in edema formation in several

neurological disorders (Simard et al., 2003, Verkman, 2008, Badaut et al., 2011b). However, the beneficial or deleterious role of AQP4 in edema formation is still unclear and depends on the pathological model (Badaut et al., 2007). Recent *in vitro* and *in vivo* studies of water diffusion in normal brain tissue have shown that AQP4 may be important in edema formation (Badaut et al., 2011a). Manley and colleagues have shown that AQP4-deficient mice have decreased lesion volume after acute water intoxication and permanent ischemia at 24 hours as compared to wild type mice (Manley et al., 2000). Notably, AQP4 has also been shown to have a role in water clearance when vasogenic edema is present (Papadopoulos et al., 2004). We have recently shown improvements in neurologic testing and physiologic measures in jTBI rats after AQP4 knockdown using small interfering RNA (siRNA) (Fukuda et al., 2013).

These findings indicate that a transient knockdown of AQP4 may improve the outcome for brain trauma patients. Despite some recent reports proposing the use of ionic channel inhibitors to block AQP4 channels (Migliati et al., 2009) and pretreatment with certain drugs (Igarashi et al., 2011), there are no specific inhibitors for AQPs available for clinical use (Sogaard and Zeuthen, 2008, Badaut et al., 2011b).

RNA Interference

Recently, RNA interference (RNAi) to transiently knockdown proteins of interest has garnered considerable attention in basic science (Soutschek et al.,

2004, Zimmermann et al., 2006) and in the clinic with some success in clinical trials using siRNA against vascular endothelial growth factor (VEGF) receptors for the treatment of cancer (Bullinger et al., 2002, Davis, 2009, Brower, 2010). RNAi selectively degrades messenger RNA (mRNA), thus silencing a specific protein gene of interest (Gonzalez-Alegre and Paulson, 2007).

siRNA are short sequences of double stranded RNA (20-23 nucleotides) that can be artificially synthesized. Previous studies have used adenovirus, lentivirus, or adenovirus-associated vectors for in vivo siRNA delivery causing additional concerns regarding patient safety (Gonzalez-Alegre and Paulson, 2007, Wood et al., 2007). These methods could potentially cause an immunologic risk for the brain, limiting its clinical potential. Using a new vector system, a cationic lipid carrier, alleviated these safety concerns by allowing for siRNA entry into the cellular cytoplasm via endocytosis (Santel et al., 2006). When inside a living cell, these short RNA molecules are incorporated into a multiprotein complex called the RNA-induced silencing complex (RISC). Using siRNA allows for inhibition of the expression of a specific protein in a sequence dependent manner.

In our group, we have recently shown the effectiveness of siRNA against AQP4 (siAQP4) to decrease brain AQP4 expression both *in vitro* and *in vivo* (Badaut et al., 2011a, Fukuda et al., 2013). siAQP4 provides a valuable method of transiently decreasing AQP4 protein levels and is especially attractive since siRNA treatment is currently in clinical trials (Tabernero et al., 2013)

Neuroimaging TBI

Comparison of clinical computed tomography (CT) and MRI scans found that MRI allows for increased detection of TBI related abnormalities (Lee et al., 2008). The use of MRI was reported in head trauma patients early in the eighties, but especially after 1986, several important studies were conducted. It has consistently been demonstrated that MRI is more sensitive than CT in detection of parenchymal lesions, diffuse axonal injury (DAI), brain stem lesions and cortical contusions (Zimmerman et al., 1986, Kelly et al., 1988, Gentry et al., 1989). Gentry et al. studied the characteristics and distribution of traumatic lesions in a series of patients with TBI, and also compared these with autopsy findings (Gentry et al., 1989). They demonstrated that the patterns of lesions depicted in the white matter with MRI were identical to what was found in the pathologic and animal studies.

There are several key MRI modalities used to diagnosis neurological diseases. One of them is diffusion-weighted imaging (DWI), which was developed in 1986 and was first reported in human TBI in 1999 (Liu et al., 1999). The method is based on adding strong and rapid magnetic field diffusion sensitizing gradients to a fast T2-weighted imaging (T2WI) sequence. This technique provides image contrast, which results from the molecular diffusion of water molecules in the brain tissue (Schaefer, 2001). Since the DWI contains both diffusion and T2- information, these images are compared to the apparent

diffusion coefficient (ADC) map which is a parametric image where the T2-effects have been eliminated while the diffusion effects remain. DWI can reliably distinguish between vasogenic edema and cytotoxic edema. ADC values in certain regions of interest can also be quantified, which is a common design in research. Previously, we have demonstrated in adults that ADC values increased after TBI in normal appearing brain regions compared to controls (Hou et al., 2007) . Studies coupled this increase in ADC after injury with spectroscopy (Mamere et al., 2009) and Glasgow Coma Scale (Brandstack et al., 2011). Recently, one study has suggested that a rim of ADC hypointensity surrounds the increased ADC region within 3 days after injury (Newcombe et al., 2013). However, this rim incorporated into the high ADC region as the lesion grew. This rim may represent a 'traumatic penumbra' that can be rescued with effective therapy.

The role of AQP4 in jTBI is largely unknown. Inhibition of AQP4 function after jTBI could prove therapeutically beneficial by preventing edema formation. To elucidate the role of AQP4 in jTBI, its function in water mobility will first be examined in the healthy juvenile brain. MRI-derived ADC values represent water mobility and alterations of this coefficient are used as an early indicator of ischemic injury (Obenaus and Ashwal, 2008). In pathological conditions, ADC values represent water movement within tissues and reduced values are thought to be associated with a decrease in extracellular space caused by cell swelling. However, this interpretation is hypothetical and has yet to be proven (Obenaus

and Ashwal, 2008). A correlation between the ADC changes and AQP4 expression has been observed in a rat model of hypoxic ischemia (Meng et al., 2004). Within 24 hours after injury, decreased AQP4 immunostaining in the ipsilateral hemisphere coincided with reduced ADC values. Recently, we showed that AQP4 in astrocytes contributes significantly to water mobility and ADC values in normal brain tissue (Badaut et al., 2011a) and after jTBI (Fukuda et al., 2013).

Chapter 1 References

Anderson-Barnes VC, Weeks SR, Tsao JW (2010) Mild traumatic brain injury update. Continuum 16:17-26.

Badaut J, Ashwal S, Adami A, Tone B, Recker R, Spagnoli D, Ternon B, Obenaus A (2011a) Brain water mobility decreases after astrocytic aquaporin-4 inhibition using RNA interference. J Cereb Blood Flow Metab 31:819-831.

Badaut J, Ashwal S, Obenaus A (2011b) Aquaporins in cerebrovascular disease: a target for treatment of brain edema? Cerebrovasc Dis 31:521-531.

Badaut J, Brunet JF, Regli L (2007) Aquaporins in the brain: from aqueduct to "multi-duct". Metab Brain Dis 22:251-263.

Betz AL, Iannotti F, Hoff JT (1989) Brain edema: a classification based on blood-brain barrier integrity. Cerebrovascular and Brain Metabolism Reviews 1:133-154.

Brandstack N, Kurki T, Hiekkanen H, Tenovuo O (2011) Diffusivity of normal-appearing tissue in acute traumatic brain injury. Clinical Neuroradiology 21:75-82.

Brower V (2010) RNA interference advances to early-stage clinical trials. J Natl Cancer Inst 102:1459-1461.

Bullinger M, Azouvi P, Brooks N, Basso A, Christensen AL, Gobiet W, Greenwood R, Hutter B, Jennett B, Maas A, Truelle JL, von Wild KR (2002) Quality of life in patients with traumatic brain injury-basic issues, assessment and recommendations. Restor Neurol Neurosci 20:111-124.

Ciurea AV, Gorgan MR, Tascu A, Sandu AM, Rizea RE (2011) Traumatic brain injury in infants and toddlers, 0-3 years old. Journal of Medicine and Life 4:234-243.

Clark RS, Kochanek PM, Schwarz MA, Schiding JK, Turner DS, Chen M, Carlos TM, Watkins SC (1996) Inducible nitric oxide synthase expression in cerebrovascular smooth muscle and neutrophils after traumatic brain injury in immature rats. Pediatr Res 39:784-790.

Davis ME (2009) The first targeted delivery of siRNA in humans via a self-assembling, cyclodextrin polymer-based nanoparticle: from concept to clinic. Mol Pharm 6:659-668.

Dobbing J, Sands J (1981) Vulnerability of developing brain not explained by cell number/cell size hypothesis. Early Human Development 5:227-231.

Faul M XL, Wald MM, Coronado VG (2010) Traumatic brain injury in the United States: emergency department visits, hospitalizations and deaths 2002-2006.: Atlanta (GA): Centers for Disease Control and Prevention, National center for Injury Prevention and Control.

Fulton JB, Yeates KO, Taylor HG, Walz NC, Wade SL (2012) Cognitive predictors of academic achievement in young children 1 year after traumatic brain injury. Neuropsychology 26:314-322.

Fukuda AM, Adami A, Pop V, Bellone JA, Coats JS, Hartman RE, Ashwal S, Obenaus A, Badaut J (2013) Posttraumatic reduction of edema with aquaporin-4 RNA interference improves acute and chronic functional recovery. J Cereb Blood Flow Metab, doi:10.1038/jcbfm.2013.118.

Gentry LR, Godersky JC, Thompson BH (1989) Traumatic brain stem injury: MR imaging. Radiology 171:177-187.

Gonzalez-Alegre P, Paulson HL (2007) Technology Insight: therapeutic RNA interference—how far from the neurology clinic? Nature Clinical Practice Neurology 3:394-404.

Gotschall CS, Papero PH, Snyder HM, Johnson DL, Sacco WJ, Eichelberger MR (1995) Comparison of three measures of injury severity in children with traumatic brain injury. J Neurotrauma 12:611-619.

Hou DJ, Tong KA, Ashwal S, Oyoyo U, Joo E, Shutter L, Obenaus A (2007) Diffusion-weighted magnetic resonance imaging improves outcome prediction in adult traumatic brain injury. J Neurotrauma 24:1558-1569.

Igarashi H, Huber VJ, Tsujita M, Nakada T (2011) Pretreatment with a novel aquaporin 4 inhibitor, TGN-020, significantly reduces ischemic cerebral edema. Neurol Sci 32:113-116.

Inglese M, Makani S, Johnson G, Cohen BA, Silver JA, Gonen O, Grossman RI (2005) Diffuse axonal injury in mild traumatic brain injury: a diffusion tensor imaging study. Journal of Neurosurgery 103:298-303.

Jennett B (1998) Epidemiology of head injury. Arch Dis Child 78:403-406.

Kelly AB, Zimmerman RD, Snow RB, Gandy SE, Heier LA, Deck MD (1988) Head trauma: comparison of MR and CT--experience in 100 patients. AJNR Am J Neuroradiol 9:699-708.

Kraus JF, Rock A, Hemyari P (1990) Brain injuries among infants, children, adolescents, and young adults. American Journal of Diseases of Children 144:684-691.

Liu AY, Maldjian JA, Bagley LJ, Sinson GP, Grossman RI (1999) Traumatic brain injury: diffusion-weighted MR imaging findings. AJNR Am J Neuroradiol 20:1636-1641.

Mamere AE, Saraiva LA, Matos AL, Carneiro AA, Santos AC (2009) Evaluation of delayed neuronal and axonal damage secondary to moderate and severe traumatic brain injury using quantitative MR imaging techniques. AJNR Am J Neuroradiol 30:947-952.

Manley GT, Fujimura M, Ma T, Noshita N, Filiz F, Bollen AW, Chan P, Verkman AS (2000) Aquaporin-4 deletion in mice reduces brain edema after acute water intoxication and ischemic stroke. Nat Med 6:159-163.

Margulies S, Hicks R (2009) Combination therapies for traumatic brain injury: prospective considerations. J Neurotrauma 26:925-939.

Meng S, Qiao M, Lin L, Del Bigio MR, Tomanek B, Tuor UI (2004) Correspondence of AQP4 expression and hypoxic-ischaemic brain oedema monitored by magnetic resonance imaging in the immature and juvenile rat. The European Journal of Neuroscience 19:2261-2269.

Migliati E, Meurice N, DuBois P, Fang JS, Somasekharan S, Beckett E, Flynn G, Yool AJ (2009) Inhibition of aquaporin-1 and aquaporin-4 water permeability by a derivative of the loop diuretic bumetanide acting at an internal pore-occluding binding site. Mol Pharmacol 76:105-112.

Morales DM, Marklund N, Lebold D, Thompson HJ, Pitkanen A, Maxwell WL, Longhi L, Laurer H, Maegele M, Neugebauer E, Graham DI, Stocchetti N, McIntosh TK (2005) Experimental models of traumatic brain injury: do we really need to build a better mousetrap? Neuroscience 136:971-989.

Moran LM, Taylor HG, Rusin J, Bangert B, Dietrich A, Nuss KE, Wright M, Minich N, Yeates KO (2012) Quality of life in pediatric mild traumatic brain injury and its relationship to postconcussive symptoms. Journal of Pediatric Psychology 37:736-744.

Newcombe VF, Williams GB, Outtrim JG, Chatfield D, Gulia Abate M, Geeraerts T, Manktelow A, Room H, Mariappen L, Hutchinson PJ, Coles JP, Menon DK (2013) Microstructural basis of contusion expansion in traumatic brain injury: insights from diffusion tensor imaging. J Cereb Blood Flow Metab 6:855-62.

Obenaus A, Ashwal S (2008) Magnetic resonance imaging in cerebral ischemia: focus on neonates. Neuropharmacology 55:271-280.

Papadopoulos MC, Manley GT, Krishna S, Verkman AS (2004) Aquaporin-4 facilitates reabsorption of excess fluid in vasogenic brain edema. FASEB J 18:1291-1293.

Reese TS, Karnovsky MJ (1967) Fine structural localization of a blood-brain barrier to exogenous peroxidase. The Journal of Cell Biology 34:207-217.

Santel A, Aleku M, Keil O, Endruschat J, Esche V, Fisch G, Dames S, Loffler K, Fechtner M, Arnold W, Giese K, Klippel A, Kaufmann J (2006) A novel siRNA-lipoplex technology for RNA interference in the mouse vascular endothelium. Gene Ther 13:1222-1234.

Schaefer PW (2001) Applications of DWI in clinical neurology. J Neurol Sci 186 Suppl 1:S25-35.

Simard M, Arcuino G, Takano T, Liu QS, Nedergaard M (2003) Signaling at the gliovascular interface. J Neurosci 23:9254-9262.

Sogaard R, Zeuthen T (2008) Test of blockers of AQP1 water permeability by a high-resolution method: no effects of tetraethylammonium ions or acetazolamide. Pflugers Arch 456:285-292.

Soutschek J, Akinc A, Bramlage B, Charisse K, Constien R, Donoghue M, Elbashir S, Geick A, Hadwiger P, Harborth J, John M, Kesavan V, Lavine G, Pandey RK, Racie T, Rajeev KG, Rohl I, Toudjarska I, Wang G, Wuschko S, Bumcrot D, Koteliansky V, Limmer S, Manoharan M, Vornlocher HP (2004) Therapeutic silencing of an endogenous gene by systemic administration of modified siRNAs. Nature 432:173-178.

Suh M, Kolster R, Sarkar R, McCandliss B, Ghajar J (2006) Deficits in predictive smooth pursuit after mild traumatic brain injury. Neurosci Lett 401:108-113.

Tabernero J, Shapiro GI, Lorusso PM, Cervantes A, Schwartz GK, Weiss GJ, Paz-Ares L, Cho DC, Infante JR, Alsina M, Gounder MM, Falzone R, Harrop J, White AC, Toudjarska I, Bumcrot D, Meyers RE, Hinkle G, Svrzikapa N, Hutabarat RM, Clausen VA, Cehelsky J, Nochur SV, Gamba-Vitalo C, Vaishnaw AK, Sah DW, Gollob JA, Burris HA, 3rd (2013) First-in-Humans Trial of an RNA Interference Therapeutic Targeting VEGF and KSP in Cancer Patients with Liver Involvement. Cancer Discovery 3:406-417.

Taylor HG, Alden J (1997) Age-related differences in outcomes following childhood brain insults: an introduction and overview. Journal of the International Neuropsychological Society : JINS 3:555-567.

Unterberg AW, Stover J, Kress B, Kiening KL (2004) Edema and brain trauma. Neuroscience 129:1021-1029.

Verkman AS (2008) Mammalian aquaporins: diverse physiological roles and potential clinical significance. Expert Reviews in Molecular Medicine 10:e13.

Wood M, Yin H, McClorey G (2007) Modulating the expression of disease genes with RNA-based therapy. PLoS Genetics 3:0845-0854.

Zimmerman RA, Bilaniuk LT, Hackney DB, Goldberg HI, Grossman RI (1986) Head injury: early results of comparing CT and high-field MR. AJR American Journal of Roentgenology 147:1215-1222.

Zimmermann TS, Lee AC, Akinc A, Bramlage B, Bumcrot D, Fedoruk MN, Harborth J, Heyes JA, Jeffs LB, John M, Judge AD, Lam K, McClintock K, Nechev LV, Palmer LR, Racie T, Rohl I, Seiffert S, Shanmugam S, Sood V, Soutschek J, Toudjarska I, Wheat AJ, Yaworski E, Zedalis W, Koteliansky V, Manoharan M, Vornlocher HP, MacLachlan I (2006) RNAi-mediated gene silencing in non-human primates. Nature 441:111-114.

Chapter 2

Characterizing Lesion Development after Traumatic Brain Injury in Juvenile Rats using Magnetic Resonance Imaging

Abstract

Age and severity are among the most significant predictors of traumatic brain injury (TBI) outcomes. Compared to the adult brain, both clinical and experimental studies reveal that the immature brain is unique in its response and vulnerability to TBI, due in part, to the developmental and structural differences of the brain's response to injury. Most investigations of TBI have utilized histopathology to characterize injury severity into mild, moderate, and severe categories. In the present study, we characterized the temporal and spatial injury after graded juvenile TBI (jTBI) *in vivo* using magnetic resonance imaging (MRI) at 6 hours, 1 and 3 days post injury. From MRI parameters studied, we found edema (T2WI) and blood volumes (SWI) to correlate with graded injuries at 6 hours and persisted through 3 days. Mild jTBI did not reveal any detectable edema at 3 days, while severe jTBI transected multiple brain regions including the corpus callosum and hippocampus in all cases. Blood deposition and neuron degeneration increased incrementally with increasing severity after 3 days. Moderate jTBI in P17 rat pups is an excellent model of TBI because it induces

sufficient edema to be analyzed for therapeutic studies, as the injury is restricted to one brain region. Future studies will attempt to use therapeutic agents that can prevent or reduce edema formation associated with jTBI.

Introduction

Traumatic brain injury (TBI) is one of the most common neurological disorders among all age groups, particularly adolescents and young adults (Gotschall et al., 1995). The most common causes of juvenile TBI (jTBI) can range from falls, sports, and motor vehicle accidents (Prins and Hovda, 2003). jTBI patients are at higher risk of life-long disability or death due in part to increased brain swelling and edema formation (Bauer and Fritz, 2004). TBI patients with moderate and severe injuries have also associated intracranial hemorrhagic injuries. However, the pathophysiology of TBI is incompletely understood, in large part because patients often present with a complexity of lesions of varying severity and regional distribution (O'Connor et al., 2011). Evaluation of these mechanisms can be critical to understanding the pathophysiology of post-traumatic neurodegeneration in jTBI and can provide new approaches for treatment.

Recently, neuroimaging has demonstrated to be an effective, noninvasive tool to diagnose TBI. More importantly, the progression of the injury can be monitored temporally in patients and animal models. Kato and colleagues have demonstrated that T2-relaxation times correlate with tissue water content and can provide insight to vasogenic edema following ischemic injury (Kato et al., 1986). In TBI experimental models, manually defined regions of interest (ROIs) revealed positive correlations between T2 relaxation values and poor histological and behavioral outcomes as well (Kharatishvili et al., 2009).

Of the various magnetic resonance imaging (MRI) modalities, susceptibility-weighted imaging (SWI) has the greatest potential to identify extravascular blood by accentuating paramagnetic properties of blood products (Haacke et al., 2004). Depending on the type and severity of brain injury, peak edema is typically observed 24-48 hours following injury and resolves by approximately 4-7 days, while hemorrhagic lesions can occur within the first 3-4 days and resolution can take months (Oehmichen et al., 2003, Obenaus et al., 2007, Kurland et al., 2012, Fukuda et al., 2013). These techniques have already been used in infants and children with brain disorders including TBI (Tong et al., 2008). However, given the lack of progress in clinical trials to treat TBI, new approaches to assess model development are warranted to achieve success at the bedside.

There are a limited number of developmental (postnatal day 17-35) jTBI models with the most commonly used being either controlled cortical impact (CCI) or fluid percussion injury (FPI). Animal models are important to elucidate lesion progression after brain injury and to establish a strategy for drug therapy before use in clinical trials. CCI and FPI have been extensively used due to motor and cognitive impairments resembling many of the behavioral deficits observed in TBI patients (Yu et al., 2009). Many studies have focused on the CCI injury due to its ease of use, reproducibility, and the ability to adjust the degree of injury severity. In the CCI model, the injury to the brain initially presents as necrotic cell death in the underlying tissue and white matter axonal injury, both

reminiscent of the clinical TBI pathology, but also followed by apoptotic cell death in surrounding tissue due to multiple subsequent events such as edema, ischemia, excitotoxicity and altered gene expression in infant (Dikranian et al., 2008, Sandhir et al., 2008) and adult mice (Sandhir et al., 2008). Despite the abundance of CCI studies, only a few studies have characterized the range of trauma severity, primarily focusing on histological evaluation in adult rodents (Igarashi et al., 2007, Yu et al., 2009). Surprisingly, all of these reports focus on adult TBI and what remains to be elucidated are the effects of graded injuries to the juvenile brain.

This study is the first to describe a postnatal day 17 (P17) juvenile model of TBI using MRI to non-invasively describe the (1) temporal extent of injury in 3 severity groups, (2) lesion composition with regard to edema and blood, and (3) best severity model for testing therapeutic agents in subsequent studies.

Methods and Experimental Design

Experiments and care of animals were conducted according to the principles and procedures of the Guidelines for Care and Use of Experimental Animals and approved by Loma Linda University. Sprague Dawley rat pups at P17 were housed in a temperature controlled (64-69^{o}F) animal facility on a 12-hour light/dark cycle.

Rat Model of Graded Juvenile TBI. Rat pups were anesthetized with isoflurane (3% induction, 2.0% maintenance) and placed in a stereotaxic

apparatus (David Kopf Instrument, Tujunga, USA). Following a midline incision over the skull, a 3 mm diameter hole was drilled over the right hemisphere centered at 1 mm posterior from bregma and 2 mm lateral to midline (-1 mm AP, -2 mm ML) using a handheld drill (Fine Science Tools Inc., Foster City, CA). The dura was left intact and any overt bleeding was lightly rinsed with saline solution. CCI injury was induced using a pneumatic impactor with a 2 mm blunt tip angled at 20 degrees to the surface of the brain. The impactor compressed the brain rapidly at 2.37 m/sec with a dwell time of 250ms. Mild, moderate, and severe jTBI was differentiated by changing the depth of compression at 1.0, 1.5, and 2.0 mm below the cortical surface. Immediately after impact, the wound was sutured with non-absorbable 5-0 silk sutures (Covidien, Mansfield, MA) and the pups then placed on a warm heating pad for recovery and returned to their dams after waking from surgery. Sham operated rat pups were treated the same but did not undergo CCI.

Magnetic Resonance Imaging and Analysis. MRI was performed at 6 hours, 1, and 3 days after CCI. After CCI, rat pups were lightly anesthetized using isoflurane (3% induction, 1% maintenance) and body temperature maintained at 36-37 ± 1^{o}C using a thermostat controlled heated water cushion. MR data was collected on a Bruker Advance 4.7T MRI containing a radio frequency coil (Bruker Biospin, Billerica MA). Using MRI, we evaluated two key parameters: 1) edema development and formation (T2-weighted imaging; T2WI), 2) localization of extravascular blood (SWI). The T2 sequence had the following

parameters: TR/TE (time to repetition/echo time) = 3,278 ms / 20 ms, matrix = 256 x 256, field of view (FOV) = 2.3 cm, 2 averages and 6 echos. The SWI sequence was acquired using the following parameters: TR/TE = 57.8 / 20 ms, flip angle = 20 degrees, matrix = 256 x 256, FOV = 2.3 cm, 23 mm slab thickness with 48 partitions. Total imaging time was 51 minutes.

T2 relaxation rates were determined for each pixel and T2 maps were generated. T2 images were analyzed using regions of hyperintensity to delineate the spatial development of the lesion volume (edema). 3D imaging software (Amira, Mercury Computer Systems, San Diego, CA) was used to extract hyperintense lesion volume, ipsi- and contralateral hemispheric brain volumes. SWI was generated from magnitude and phase data sets using in-house Spin image processing software (The MRI Institute for Biomedical Research, Detroit, MI). SWI has been used as a noninvasive technique to evaluate extravascular blood. Analysis in Amira included lesion volume (hypointensities) data from the SWI images. The edema lesion volume, determined using T2WI, was divided by the sum of both hemisphere volumes (from T2WI) to obtain percent edema lesion to correct for individual brain differences. The blood lesion volume was calculated in the same manner except SWI was used to determine blood volume. The blood volume was then divided by the sum of both hemisphere volumes (from T2 images) to obtain percent lesion to correct for individual brain size differences.

Histology. After imaging, all animals were transcardially perfused with 4% paraformaldehyde and put in 30% sucrose in phosphate buffered saline (PBS)

for cryoprotection before freezing and cutting on a cryostat. All staining was performed on 30 µm sections centered at the lesion site 3 days post jTBI. Prussian blue staining was performed as previously described to detect extravascular blood within the tissue (Obenaus et al., 2011). Degenerating neurons were detected using Fluoro-Jade B (Millipore, Temecula, CA) staining on thawed tissue sections as previously described (Schmued and Hopkins, 2000). The number of damaged neurons (Fluoro-Jade B) within the tissue was quantified using ImageJ software (ITCN plugin, US National Institutes of Health, Bethesda, MD). Two adjacent sections from each rat pup were imported into ImageJ and converted to 8 bit and inverted. Four primary regions of interest (ROIs) including lesion, perilesion, ipsi- and contralateral corpus callosum were delineated on the two adjacent sections. ITCN plugin was used to detect dark peaks in the selected ROI. The number of Fluoro-Jade B positive cells was quantified by averaging the number of positive cells from the two sections. To determine the number of Fluoro-Jade B positive neurons in the ipsilateral cortex, the number of neurons in lesion and perilesion were summed. The total number of Fluoro-Jade B positive cells for each pup was calculated by combining all four ROIs.

Statistics. Using SigmaPlot (Systat Software Inc., San Jose, CA), MRI blood, edema volume data, and Fluoro-Jade staining were analyzed by one-way analysis of variance with post hoc Bonferroni test. An α-level of 0.05 was used for all statistical significance tests. All data are expressed as the mean ± SEM.

Results

Graded jTBI Severity at 6 hours. CCI injury resulted in increasing lesion volume with increasing depth of cortical compression at 6 hours (Fig. 2.1). The impact site could be seen on both T2 and SWI in jTBI pups (Fig. 2.1, arrows). There was no visible lesion due to the craniotomy in sham pups (Fig. 2.1, line). Severe jTBI usually resulted in hippocampal involvement (100% of animals) compared to 60% in moderate and never in mild jTBI. SWI sensitivity to blood makes it an ideal modality to visualize injury in the juvenile brain.

CCI Depth Distance Increases Early Edema Formation. To evaluate edema formation, we used T2 images at 6 hours, 1 and 3 days to quantify edema lesion volume. Shams did not have detectable edema volumes across any time points. Mild jTBI (1.0 mm depth) resulted in 0.11% ± 0.04 edema volume of the total brain at 6 hours, which was almost undetectable at 3 days (0.004% ± 0.01) (Fig. 2.2). Edema lesion volume was 0.51% ± 0.04 after moderate jTBI at 6 hours. At 3 days, the edema volume had decreased 73% to 0.15% ± 0.03 compared to 1 day ($p < 0.05$). Severe jTBI rat pups started with the highest percentage of edema volumes at 0.83% ± 0.09 at 6 hours. Similar to mild and moderate jTBI pups, severe edema volume decreased 61% by 3 days to 0.32% ± 0.05 ($p < 0.05$). Lastly, there was a significant difference in the interaction between severity groups and time ($p < 0.04$).

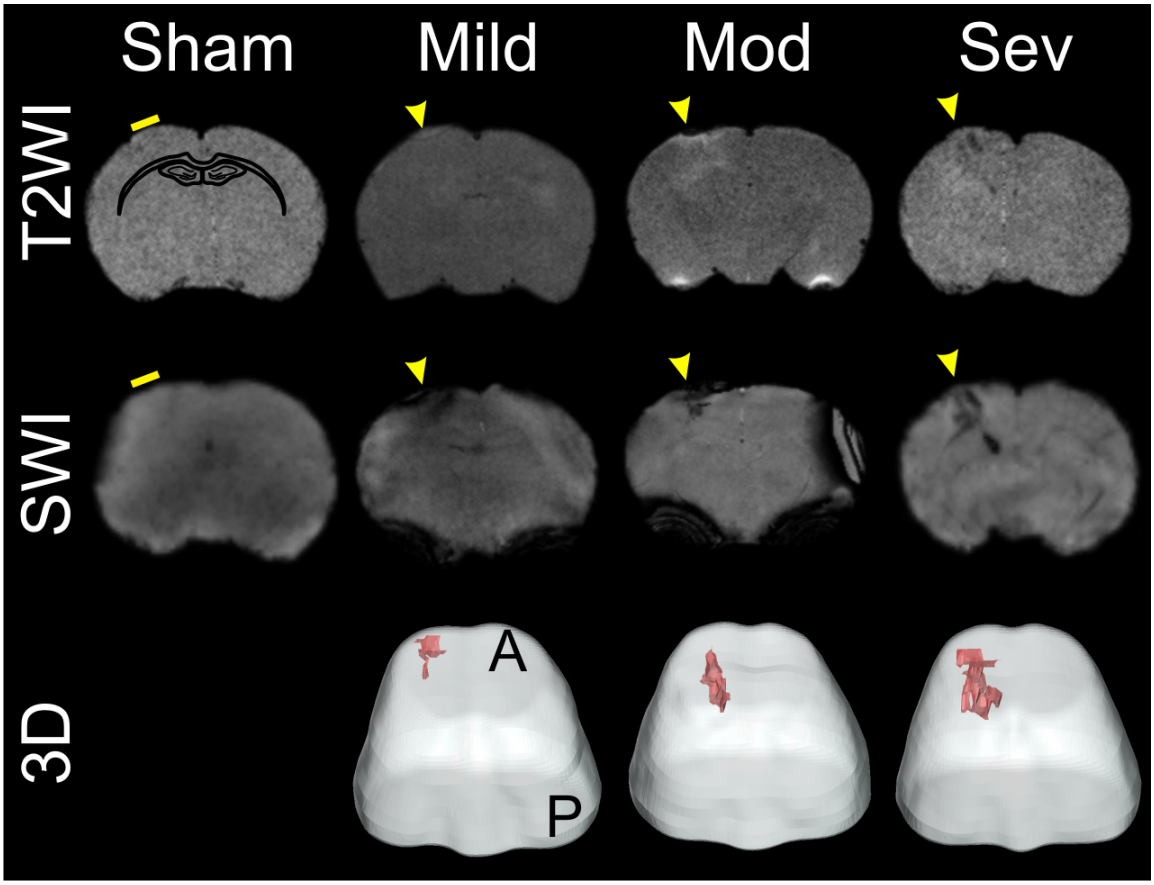

Figure 2.1: Multi-modal MRI Assessments of Traumatic Injury at 6 hours after Graded jTBI Severity.

Representative T2WI, SWI and 3D reconstruction images from CCI injury resulting in an increase in lesion volume with increasing severity at 6 hours. Impact site can be seen on both T2WI and SWI in jTBI pups (arrows). There is no visible lesion due to the craniotomy in sham pups (line). 3D reconstruction of the injured brain where red denotes the lesion volume and white denotes normal appearing brain matter. Severe jTBI often resulted in hippocampal involvement in 100% of animals compared to 60% in moderate and 0% in mild jTBI. Abbreviations: A=anterior, P=posterior, Mod = moderate, Sev = severe

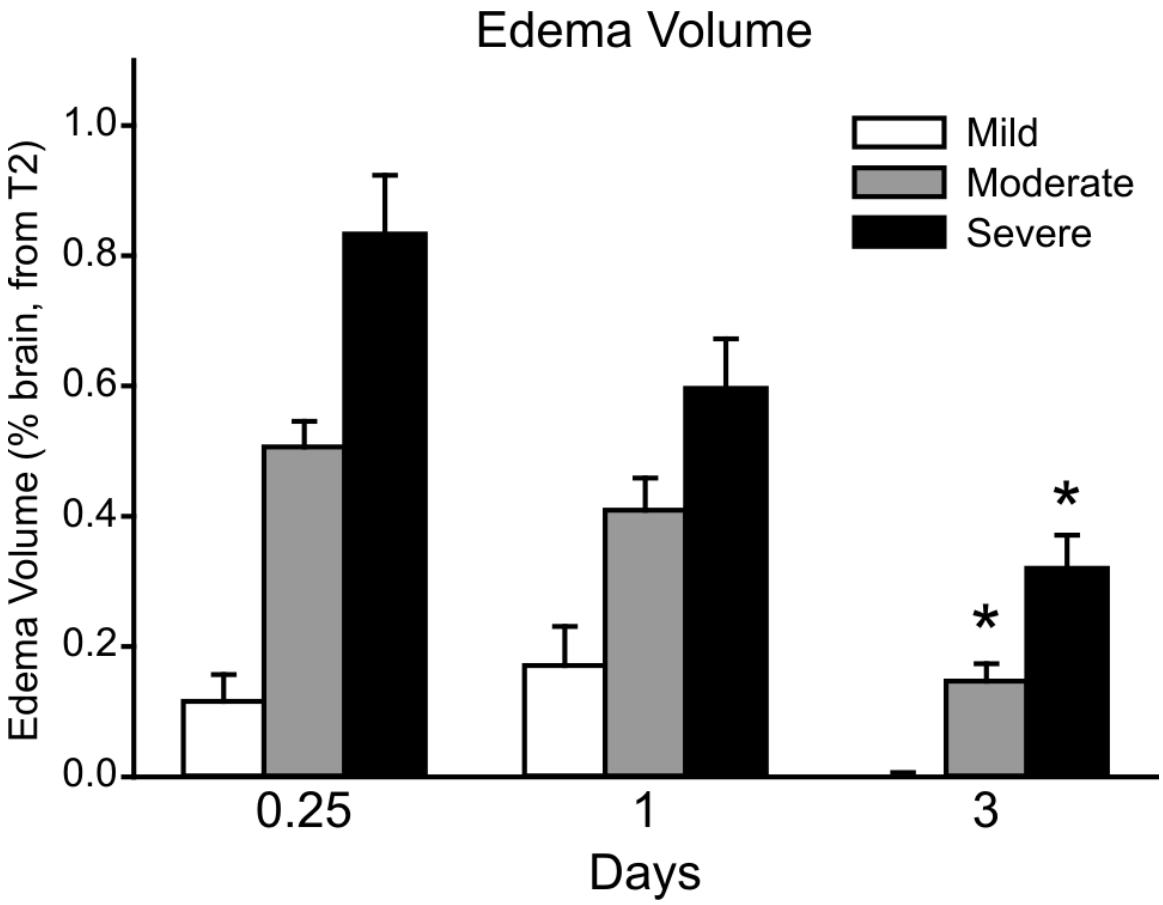

Figure 2.2: Edema Volume Increases with jTBI Severity

There was a significant interaction between severity groups and time points ($p < 0.04$). Shams did not have detectable edema volumes across all time points. Mild jTBI resulted in edema volume that was 0.11% ± 0.04 of brain volume at 6 hours, which was decreased to 0.004% ± 0.01 at 3 days. Edema volume was 0.51% ± 0.04 of the brain after moderate jTBI at 6 hours. At 3 days, the edema volume had decreased 73% to 0.15% ± 0.03 compared to 6 hours ($p < 0.05$). Severe jTBi rat pups started with the highest percentage of edema volume at 0.83% ± 0.09 at 6 hours. Similar to mild and moderate jTBI pups, severe edema volume decreased 61% by 3 days to 0.32% ± 0.05 ($p < 0.05$).

All together, these data suggest that our model of varying severities resulted in graded edema volumes. Interestingly, edema volumes significantly decreased from 1 to 3 days in mild and moderate jTBI. However, mild jTBI resulted in almost no detectable edema volume at 3 days, making moderate or severe jTBI the most likely candidate for therapeutic investigations against detectable edema formation.

Blood Volume stays Relatively Unchanged after 3 days. To evaluate blood lesion volume after jTBI, we quantified hypointensities on SWI. Sham surgery resulted in a 0.07% ± 0.01 at 6 hours, which decreased at 1 day to 0.00%. Mild jTBI resulted in 0.08% ± 0.07 at 6 hours (Fig. 2.3). At 1 day, blood volume decreased briefly by 38% but then increased to 0.09% ± 0.15 of the whole brain at 3 days. A similar pattern was observed after moderate jTBI. At 6 hours, the resulting blood volume was 0.33% ± 0.09. At 1 day, this blood volume quickly decreased to 0.29% ± 0.07 of the brain, before increasing to 0.32% ± 0.02 at 3 days. Similar to edema lesion volumes, severe jTBI pups started with the highest blood volume at 0.85% ± 0.20 at 6 hours. The blood volume sustained the same profile from the mild and moderate pups, decreasing at 1 day (0.51% ± 0.35) and returning to 0.085% ± 0.14 at 3 days. There was a significant difference between each group at each time point ($p < 0.001$), but there was no significance seen across time points.

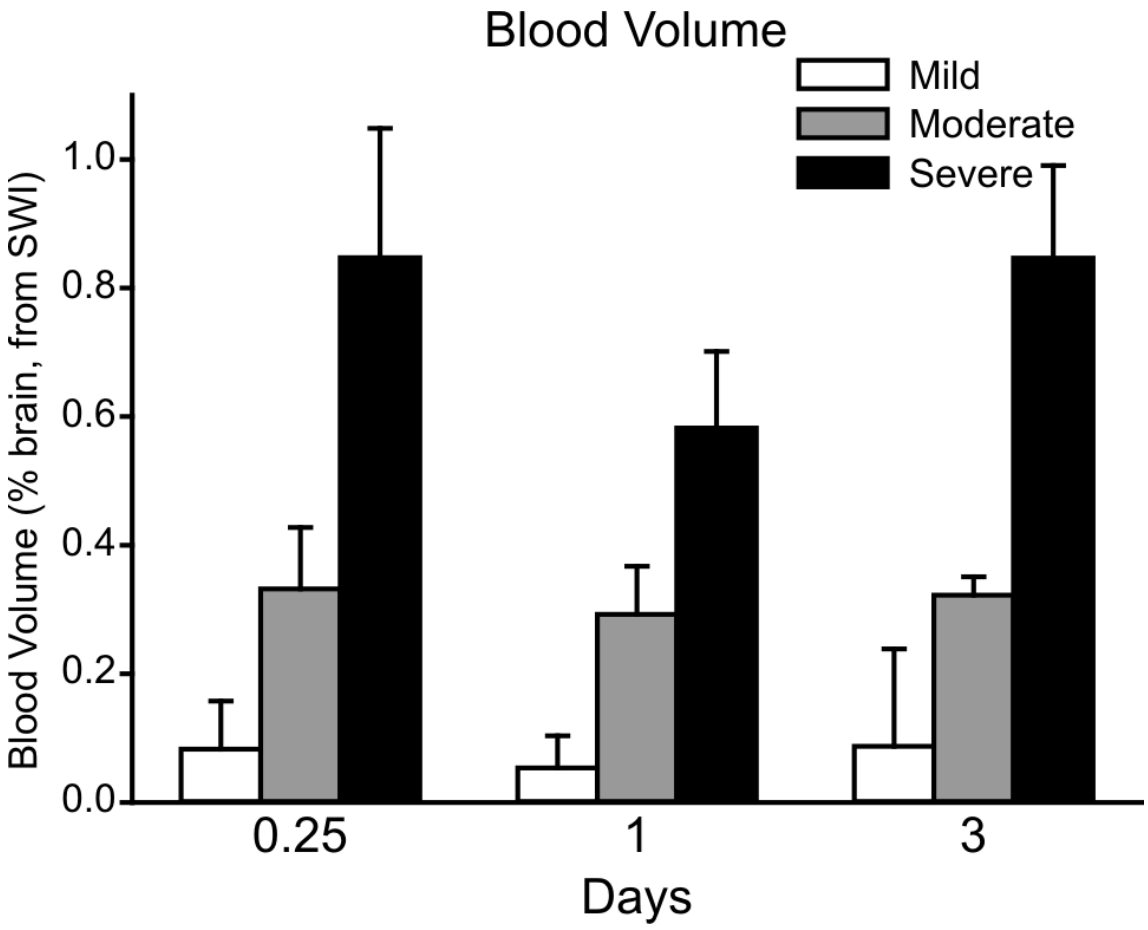

Figure 2.3: Blood Volume Increases with Compression Depth

There was a significant difference between each group at each time point ($p < 0001$). Sham surgery resulted in a blood volume that was 0.007% ± 0.001 of the total brain volume at 6 hours, which decreased by 1 day to 0.00%. Mild jTBI resulted in a blood volume that was 0.08% ± 0.07 of the brain at 6 hours. At 1 day, this blood volume decreased briefly by 38% but then increased to a final volume of 0.09% ± 0.15 of the whole brain at 3 days. At 6 hours, moderate jTBI blood volume was 0.33% ± 0.09 of the brain. At 1 day, this blood volume quickly decreased to 0.29% ± 0.07 of the brain, before increasing to 0.32% ± 0.02 at 3 days. Similar to edema lesion volumes, severe jTBI pups started with the highest blood volume at 0.85% ± 0.20 of the brain at 6 hours. The blood volume decreased to 0.58% ± 0.12 at 1 day but returned to 0.85% ± 0.14 after 3 days.

Lesion Composition Mostly Edema within 1 day. To evaluate the relationship between edema and blood volumes, we quantified the overall lesion composition devoted to blood or edema. We found that each severity of jTBI lesion volume comprised of ~60% edema and ~40% blood at 6 hours (Fig. 2.4). This proportion stayed relatively the same across all groups until 3 days. Mild jTBI resulted in nearly 95.7% blood at 3 days. This is likely due to the resolution of the bulk of the edema in the mild jTBI rat pups. The proportion of blood from moderate and severe jTBI pups stayed below 70% of the total lesion as the edema resolved at a much slower pace.

Absolute blood volumes taken as a percentage from the whole brain clearly illustrate the importance of blood deposition in the brain at 6 hours. Regardless of edema volume at 6 hours, blood volume seems to be indicative of jTBI severity. As seen in Figure 2.4, blood volume at 6 hours was highest after severe jTBI and lowest after mild jTBI (apart from shams). This graded blood volume led to no visible edema lesion at 3 days after mild jTBI. Taken together, blood volume as a percentage of brain volume, not a percentage of lesion, is predictive of edema resolution at 3 days.

Blood Deposition in the Distant Corpus Callosum after Severe jTBI. Prussian blue staining for extravascular blood at the site of the lesions was performed 3 days post jTBI and supported our MRI analysis, demonstrating increased blood deposition within the ipsilateral cortex and corpus callosum with worsening jTBI severity. Blood deposition appeared concentrated at the impact

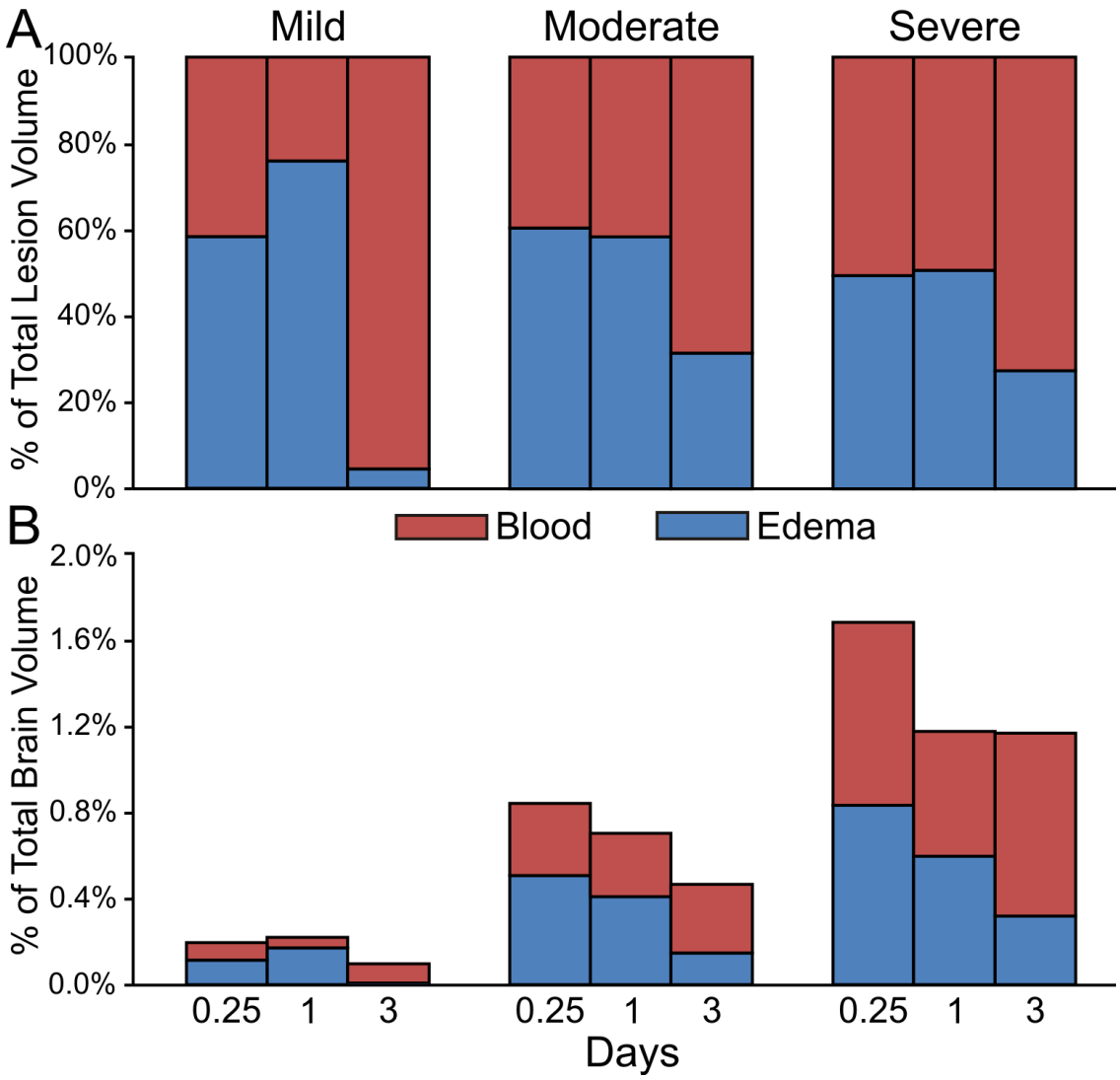

Figure 2.4: Lesion Composition after jTBI

A. The severity of jTBI lesion volume was comprised of ~60% edema and ~40% blood at 6 hours. Mild jTBI resulted in nearly 95.7% blood at 3 days. Proportion of blood from moderate and severe jTBI stayed below 70% of the total lesion as the edema resolved at a much slower pace at 1 and 3 days. B. Blood volume at 6 hours was highest after severe jTBI and lowest after mild jTBI (apart from shams). Total lesion volume (blood + edema) after mild jTBI was 0.19%. Lesion volumes increased with severity to 0.84% after moderate jTBI and 1.68% after severe jTBI.

site within the mild jTBI group, while the moderate and severe had a more diffuse deposition (Fig. 2.5A-B). Prussian blue positive staining in the contralateral corpus callosum was not detected in any mild rat pups, but was detected in 25% and 75% of all moderate and severe jTBI rat pups, respectively (Fig. 2.5C).

Degenerating Neurons Increase with Increasing Severity. A substantial number of Fluoro-Jade positive cell-bodies were observed at the site of the impact suggesting ongoing neuronal degradation (Fig. 2.6A). In the lesion and perilesion, there were approximately 3.2 times more Fluoro-Jade positive cells after moderate jTBI compared to mild and 1.8 times more after severe compared to moderate jTBI (Fig. 2.6B, $p < 0.001$). This profile is also observed when counting Fluoro-Jade positive cells in the ipsi- and contralateral corpus callosum (84 ± 32 mild vs. 145 ± 21 moderate vs. 217 ± 31 severe, $p < 0.032$). Total Fluoro-Jade cell counts revealed an almost doubling of degenerating neurons from mild to moderate to severe (179 ± 25 mild vs. 481 ± 79 moderate vs. 837 ± 72 severe, $p < 0.001$).

Discussion

The juvenile rodent CCI model produced animals with reproducible graded injury severity, which is essential for future therapeutic investigations. The novel findings of this study are (1) moderate jTBI should be considered the model used for future therapeutic intervention, (2) blood volume, represented as a percent of brain volume, at 6 hours is indicative of severity, and (3) while total lesion

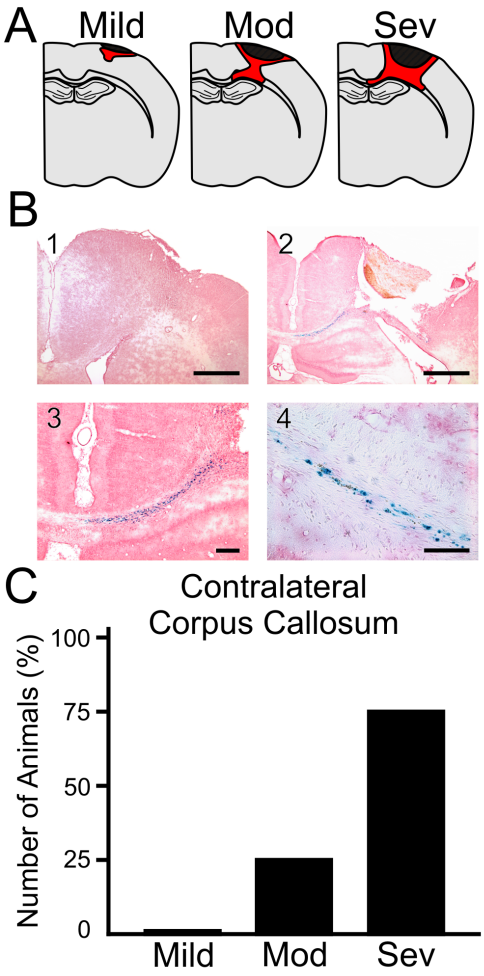

Figure 2.5: Abnormal Blood Deposition after TBI at 3 days

A. Prussian blue staining was observed in the ipsilateral cortex in all jTBI groups 3 days post injury. There was an increase in lesion size and blood deposition in the corpus callosum (red) after moderate (Mod) and severe (Sev) jTBI. This extended into the contralateral corpus callosum only after severe injury. Black denotes the TBI-induced cavitation of the tissue. B. After mild jTBI, Prussian blue staining was only detected proximal to the injury (B1). Increased blood deposition was observed in the ipsilateral (B2, higher magnification B3) and contralateral corpus callosum (B4) at the site of maximal lesion after severe jTBI. C. No Prussian blue staining was observed in the contralateral corpus callosum after mild jTBI. Only 25% of moderate jTBI pups had positive Prussian blue staining in the contralateral corpus callosum, where as 75% of severe jTBI rat pups had positive Prussian blue staining. Scale bars: B1, B2 = 1 mm; B3, B4 = 100 μm

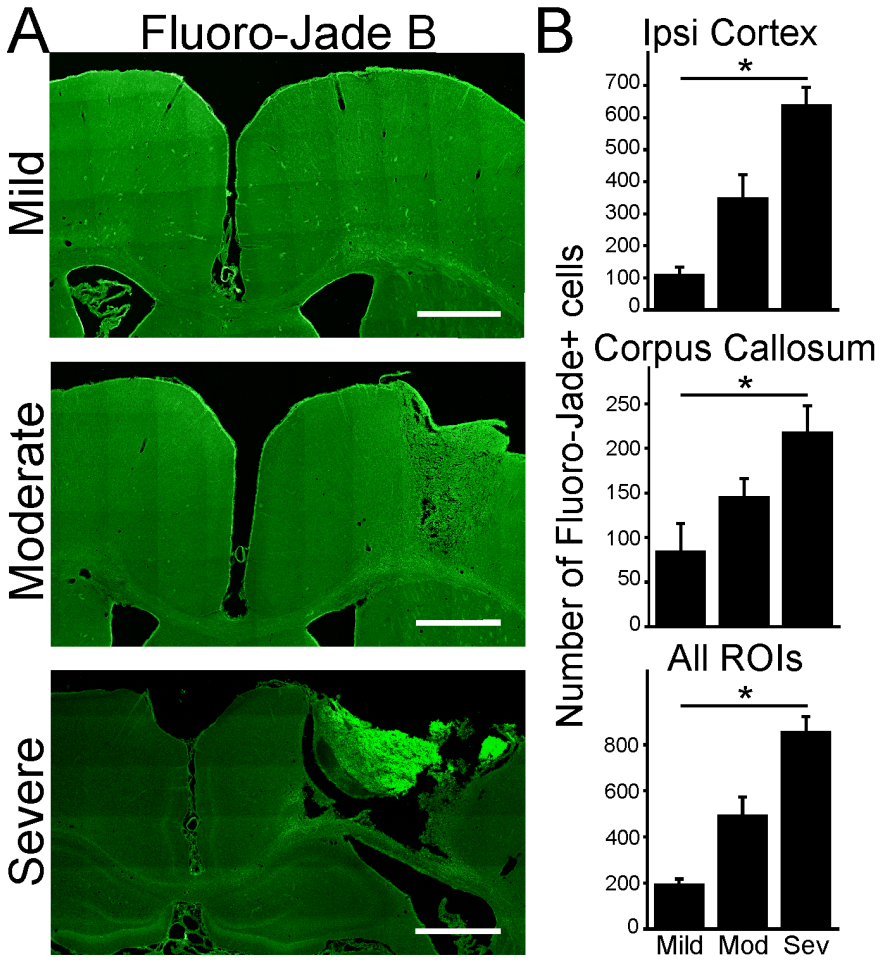

Figure 2.6: Graded Fluoro-Jade Staining after TBI at 3 days

A. Representative Fluoro-Jade B (green) images after mild, moderate (Mod), and severe (Sev) jTBI 3 days post injury illustrate the localization of degenerating neurons at the site of maximal injury. Increased number of Fluoro-Jade B positive cell bodies and staining intensity was observed in the lesion after severe jTBI compared to mild and moderate jTBI. Fluoro-Jade B staining increased incrementally with increasing severity in the corpus callosum B. Degenerating neurons were quantified using Fluoro-Jade B staining. Fluoro-Jade B positive cells significantly increased with increased jTBI severity in the ipsilateral (ipsi) cortex ($p < 0.001$) and ipsi- and contralateral corpus callosum ($p < 0.032$). The total number of Fluoro-Jade B positive cells observed when all regions of interests (ROIs) were combined revealed an approximate doubling of degenerating neurons with each worsening severity ($p < 0.001$). Scale bars: A = 1 mm

volumes are larger with increasing severity, lesion composition (percentage of blood and edema) is the same across severities early after injury. Our results strongly suggest a potential future for this model in the development of therapeutic interventions.

Until now, the noninvasive evaluation of lesion composition after TBI has largely been unexplored. Physicians have recognized that no two brain injuries are the same, underscoring the heterogeneous pathophysiology of the disease (Borlongan, 2009). CCI has been one of the most widely used injury models of TBI (Yu et al., 2009) and assessment of therapeutics across a range of TBI severities is postulated to allow for insight on the potential target patient population, thereby increasing the likelihood of success in translating laboratory findings into clinical use. Additionally, the standardization of categorization of injury severites in jTBI rodent models may aid in direct comparison between research studies, thereby helping to develop patient protocols for future therapy. To our knowledge, only one other study categorized animals into injury severities and used histology to do so, preventing the examination of temporal changes on neurological outcome (Yu et al., 2009).

While previous studies have utilized invasive histology to characterize injury severity after TBI, this study is novel in that it used noninvasive methods to categorize injury severity (Yu et al., 2009). The present observations not only mirrored previous imaging results (Immonen et al., 2009, Kharatishvili et al., 2009), but also revealed that edema and blood volumes closely tracked the TBI

severity pattern in that animals presenting the larger volume of damaged tissue exhibited the most extravascular blood deposition (Fig. 2.2-5). The observed changes in edema volume over time in rats mirrored the changes in edema volume in human patients (Obenaus and Ashwal, 2008, Chastain et al., 2009, Badaut et al., 2011). Our results also mirrored those of a study examining AQP4; this study found an increase in brain edema and AQP4 expression after closed-head TBI in adult rats (Shenaq et al., 2012). They also demonstrated decreased brain edema and neuronal cell death after inhibition of AQP4 with intravenous anti-AQP4 antibodies. In addition, a study examining brain edema and hemorrhage using MRI in a model of TBI in adult rabbits found that hemorrhage volume and edema volume correlated with functional outcome at 30 days (Li et al., 2011). At 6 hours, we found the largest differences in edema volume across severities. Mild jTBI resulted in nearly 95.7% blood at 3 days due to the resolution of most of the edema in mild jTBI rat pups. This data suggested that mild jTBI might not cause sufficient injury to evaluate therapeutic agents against edema formation.

Our data revealed that SWI-identified blood increased with CCI-induced graded jTBI severity and confirmed by histology (Fig. 2.3 and 2.5). SWI has been shown to provide a sensitive imaging modality for detecting abnormalities in blood accumulation within the brain including micro-bleeds (Haacke et al., 2010). We found that blood lesion volumes increased with compression depth when evaluated using SWI. At 3 days, there was no significance in lesion volume

compared to 6 hours, suggesting longer recovery for blood deposition compared to edema. Studies have shown a important role for vascular integrity in the mediation of brain injury (Shlosberg et al., 2010). Complementary to SWI, T2WI enables application of neuroimaging biomarkers to evaluate extravascular blood and its relation to brain injury.

MRI also shed light on the regions affected by CCI. Each brain region may respond/recover differently to injury thus a single region to test preliminary therapeutic interventions are ideal. All severe jTBI resulted in hippocampal damage, making this group less desirable as a model to test future therapies. Given this, we found that moderate jTBI is an excellent model for preclinical testing of therapeutic agents.

Prussian blue and Fluoro-Jade staining revealed tissue abnormalities ventral to the site of impact at 3 days. Blood deposition and the number of dying cells increased with deeper impact compression. Prussian blue staining characteristics closely mirrored MRI SWI blood volume data suggesting that our noninvasive methods accurately quantified extravascular blood (Fig. 2.4B and 2.5). Interestingly, Fluoro-Jade B quantification mirrored Prussian blue staining characteristics only in the ipsilateral hemisphere. Increased Fluoro-Jade positive cells coincided with increased Prussian blue area after jTBI. However, there were no significant differences observed in the number of Fluoro-Jade positive cells in the contralateral corpus callosum across all groups, even though we detected Prussian blue staining after severe jTBI at 3 days. This may be due to delayed

cell death after extravascular blood deposition in the brain parenchyma. While other studies have qualitatively described cell death after TBI in adult rats (Kharatishvili et al., 2009, Hawkins et al., 2013) and swine (Manley et al., 2006), this study is the first to our knowledge to quantitatively describe the relationship between increasing injury severity, cell death, and hemorrhage volume.

Here, we provided convincing noninvasive assessment on the relationships between abnormal blood accumulation post injury and the severity of brain injury as determined by blood and edema volume. We also anticipated that the age-specific blood-mediated pathology would be more severe after juvenile compared to adult TBI, demonstrating a developmental sensitivity. No single animal model is entirely successful in reproducing the complete spectrum of pathological changes observed after TBI and further research is necessary to fully reveal the acute and chronic changes that occur after TBI.

Chapter 2 References

Badaut J, Ashwal S, Obenaus A (2011) Aquaporins in cerebrovascular disease: a target for treatment of brain edema? Cerebrovasc Dis 31:521-531.

Bauer R, Fritz H (2004) Pathophysiology of traumatic injury in the developing brain: an introduction and short update. Experimental and Toxicologic Pathology 56:65-73.

Borlongan CV (2009) Cell therapy for stroke: remaining issues to address before embarking on clinical trials. Stroke 40:S146-148.

Chastain CA, Oyoyo UE, Zipperman M, Joo E, Ashwal S, Shutter LA, Tong KA (2009) Predicting outcomes of traumatic brain injury by imaging modality and injury distribution. J Neurotrauma 26:1183-1196.

Dikranian K, Cohen R, Mac Donald C, Pan Y, Brakefield D, Bayly P, Parsadanian A (2008) Mild traumatic brain injury to the infant mouse causes robust white matter axonal degeneration which precedes apoptotic death of cortical and thalamic neurons. Exp Neurol 211:551-560.

Fukuda AM, Adami A, Pop V, Bellone JA, Coats JS, Hartman RE, Ashwal S, Obenaus A, Badaut J (2013) Posttraumatic reduction of edema with aquaporin-4 RNA interference improves acute and chronic functional recovery. J Cereb Blood Flow Metab, doi:10.1038/jcbfm.2013.118.

Gotschall CS, Papero PH, Snyder HM, Johnson DL, Sacco WJ, Eichelberger MR (1995) Comparison of three measures of injury severity in children with traumatic brain injury. J Neurotrauma 12:611-619.

Haacke EM, Garbern J, Miao Y, Habib C, Liu M (2010) Iron stores and cerebral veins in MS studied by susceptibility weighted imaging. International Angiology 29:149-157.

Haacke EM, Xu Y, Cheng YC, Reichenbach JR (2004) Susceptibility weighted imaging (SWI). Magn Reson Med 52:612-618.

Hawkins BE, Cowart JC, Parsley MA, Capra BA, Eidson KA, Hellmich HL, Dewitt DS, Prough DS (2013) Effects of trauma, hemorrhage and resuscitation in aged rats. Brain Res 1496:28-35.

Igarashi T, Potts MB, Noble-Haeusslein LJ (2007) Injury severity determines Purkinje cell loss and microglial activation in the cerebellum after cortical contusion injury. Exp Neurol 203:258-268.

Immonen RJ, Kharatishvili I, Gröhn H, Pitkänen A, Gröhn OHJ (2009) Quantitative MRI predicts long-term structural and functional outcome after experimental traumatic brain injury. Neuroimage 45:1-9.

Kato H, Kogure K, Ohtomo H, Izumiyama M, Tobita M, Matsui S, Yamamoto E, Kohno H, Ikebe Y, Watanabe T (1986) Characterization of experimental ischemic brain edema utilizing proton nuclear magnetic resonance imaging. J Cereb Blood Flow Metab 6:212-221.

Kharatishvili I, Sierra A, Immonen RJ, Grohn OH, Pitkanen A (2009) Quantitative T2 mapping as a potential marker for the initial assessment of the severity of damage after traumatic brain injury in rat. Exp Neurol 217:154-164.

Kurland D, Hong C, Aarabi B, Gerzanich V, Simard JM (2012) Hemorrhagic progression of a contusion after traumatic brain injury: a review. J Neurotrauma 29:19-31.

Li YH, Wang JB, Li MH, Li WB, Wang D (2011) Quantification of brain edema and hemorrhage by MRI after experimental traumatic brain injury in rabbits predicts subsequent functional outcome. Neurological sciences : the Italian Neurological Society and of the Italian Society of Clinical Neurophysiology 4:731-40.

Manley GT, Rosenthal G, Lam M, Morabito D, Yan D, Derugin N, Bollen A, Knudson MM, Panter SS (2006) Controlled cortical impact in swine: pathophysiology and biomechanics. J Neurotrauma 23:128-139.

O'Connor WT, Smyth A, Gilchrist MD (2011) Animal models of traumatic brain injury: a critical evaluation. Pharmacol Ther 130:106-113.

Obenaus A, Ashwal S (2008) Magnetic resonance imaging in cerebral ischemia: focus on neonates. Neuropharmacology 55:271-280.

Obenaus A, Dilmac N, Tone B, Tian HR, Hartman R, Digicaylioglu M, Snyder EY, Ashwal S (2011) Long-term magnetic resonance imaging of stem cells in neonatal ischemic injury. Ann Neurol 69:282-291.

Obenaus A, Robbins M, Blanco G, Galloway NR, Snissarenko E, Gillard E, Lee S, Curras-Collazo M (2007) Multi-modal magnetic resonance imaging alterations in two rat models of mild neurotrauma. J Neurotrauma 24:1147-1160.

Oehmichen M, Walter T, Meissner C, Friedrich HJ (2003) Time course of cortical hemorrhages after closed traumatic brain injury: statistical analysis of posttraumatic histomorphological alterations. J Neurotrauma 20:87-103.

Prins ML, Hovda DA (2003) Developing experimental models to address traumatic brain injury in children. J Neurotrauma 20:123-137.

Sandhir R, Onyszchuk G, Berman NE (2008) Exacerbated glial response in the aged mouse hippocampus following controlled cortical impact injury. Exp Neurol 213:372-380.

Schmued LC, Hopkins KJ (2000) Fluoro-Jade: novel fluorochromes for detecting toxicant-induced neuronal degeneration. Toxicologic Pathology 28:91-99.

Shenaq M, Kassem H, Peng C, Schafer S, Ding JY, Fredrickson V, Guthikonda M, Kreipke CW, Rafols JA, Ding Y (2012) Neuronal damage and functional deficits are ameliorated by inhibition of aquaporin and HIF1alpha after traumatic brain injury (TBI). J Neurol Sci 323:134-140.

Shlosberg D, Benifla M, Kaufer D, Friedman A (2010) Blood–brain barrier breakdown as a therapeutic target in traumatic brain injury. Nature Reviews Neurology 6:393-403.

Tong KA, Ashwal S, Obenaus A, Nickerson JP, Kido D, Haacke EM (2008) Susceptibility-weighted MR imaging: a review of clinical applications in children. AJNR Am J Neuroradiol 29:9-17.

Yu S, Kaneko Y, Bae E, Stahl CE, Wang Y, van Loveren H, Sanberg PR, Borlongan CV (2009) Severity of controlled cortical impact traumatic brain injury in rats and mice dictates degree of behavioral deficits. Brain Res 1287:157-163.

Chapter 3

Brain Water Mobility Decreases after Astrocytic Aquaporin-4 Inhibition using RNA Interference

Abstract

Neuroimaging with diffusion-weighted imaging (DWI) is routinely used for clinical diagnosis/prognosis. Its quantitative parameter, the apparent diffusion coefficient (ADC), is thought to reflect water mobility in brain tissues. After injury, reduced ADC values are thought to be a consequence of decreases in the extracellular space caused by cell swelling. However, the physiological mechanisms associated with these reduced ADC values remain uncertain. Aquaporins (AQPs) facilitate water diffusion through the plasma membrane and provide a unique opportunity to examine the molecular mechanisms underlying water mobility. Because of this critical role and the recognition that brain AQP4 is distributed within astrocytic cell membranes, we hypothesized that AQP4 contributes to the regulation of water diffusion and variations in its expression would alter ADC values in the normal juvenile brain. Using RNA interference in the juvenile rodent brain, we acutely knocked down AQP4 expression and observed that a 27% AQP4-specific silencing induced a 50% decrease in ADC values, without modification of tissue structure. Our results demonstrate that

ADC values in normal brain are modulated by astrocytic AQP4. These findings have major clinical relevance as they suggest that imaging changes seen in acute neurologic disorders such as stroke and trauma in part due to changes in tissue AQP4 levels.

Introduction

Water channels (aquaporins, AQPs) facilitate water diffusion through the plasma membrane and open new avenues for understanding the molecular underpinnings of water movement in mammalian tissues (Tait et al., 2008). These channels are widely distributed in several tissues, and brain aquaporin-4 (AQP4) has been found to be highly expressed with a preferential location within astrocytic cell membranes in contact with blood vessels (Badaut et al., 2002). Several studies have already shown that AQP4 is important in edema formation and resolution after acute brain injury in various disorders, including stroke and water intoxication (Manley et al., 2000, Tait et al., 2008, Hirt et al., 2009).

In vitro astrocyte culture experiments have shown that AQP4 is involved in water movement across the cell membrane (Nicchia et al., 2003). So far, the involvement of AQP4 in cellular water mobility has not been explored *in vivo* in normal brain. The apparent diffusion coefficient (ADC) value measured using magnetic resonance imaging (MRI) represents water mobility within tissue (Le Bihan, 2003). Water diffusion can be extracellular, intracellular, and transcellular through cell membranes, and the ADC value likely reflects all three components. Alterations of this coefficient are often used as an early indicator of ischemic injury (Obenaus and Ashwal, 2008). MRI is used for the clinical evaluation and assessment of treatment in many neurologic disorders and more recently as an early indicator of brain activation during functional MRI studies (Le Bihan, 2007).

ADC values represent water movement within tissues and in pathological conditions, reduced values are thought to be associated with decreases in the extracellular space as a result of cell swelling. This interpretation is hypothetical and the underlying physiological basis of the ADC remains incompletely understood (Obenaus and Ashwal, 2008). A correlation between the ADC changes and AQP4 expression has been observed in rat models of hypoxic ischemic (Meng et al, 2004), hydrocephalic (Tourdias et al, 2009), and traumatic brain injuries (Fukuda et al., 2013). These results suggest indirectly that ADC values correlate to the level of AQP4 expression under pathological conditions. Therefore, we hypothesized that AQP4 expression in astrocytes contributes significantly to water diffusion and ADC values in normal brain tissues. This hypothesis has never been directly tested in normal brain, and to address this question, we used RNA interference, to acutely knockdown AQP4 expression in the rat brain and evaluated brain ADC changes.

Methods and Experimental Design

In vitro experiments described in the present work were approved by the Animal Care and Use Committee of the University of Lausanne. In vivo animal studies were conducted according to the principles and procedures of the Guidelines for Care and Use of Experimental Animals and were approved by Loma Linda University.

Small Interfering RNA Preparation. Our AQP4 silencing protocol was adapted from a previous publication (Saadoun et al, 2005). SMART pool® containing four small interfering RNA (siRNA) duplexes against AQP4 (400ng, siAQP4, Dharmacon Research) were mixed with 2.5 μL of interferin® (Polypus-transfection, Illkirch, France) and diluted in a saline solution (0.9%) containing 5% glucose for a final volume of 5 μL. For controls, non-targeted siRNA (siGLO RISC-free control siRNA, Thermo Fisher Scientific, Lafayette, CO) were used to monitor non-specific effects of siRNA injection. siGLO was prepared using the same protocol as siAQP4. These reagents were incubated on ice for 20 min for complex formation before injection. Sequences of siAQP4 in the SMART pool were submitted to a BLAST search to avoid the possible targeting of other genes present in brain.

Rat Surgery and Small Interfering RNA Injection. Male Sprague–Dawley rats pups (Charles River, San Diego, CA, USA) were used at post-natal day 17 (P17, n=22). Rat pups were housed with their dam in a plastic cage in a room with controlled temperature and on a 12 hour light/dark cycle. Pups were allowed to acclimatize for 7 days with food and water provided ad libitum.

For intracortical injection, rats were anesthetized with 3% isoflurane and placed in a stereotaxic apparatus (David Kopf Instrument, Tujunga, CA, USA). A sterile 22-gauge needle on a Hamilton syringe was used for injection of siRNA into the right frontal cortex with coordinates of 0.0 mm posterior to the bregma, 1.0 mm lateral to the midline, and 1.0 mm to the surface of the skull (Fig 3.1A).

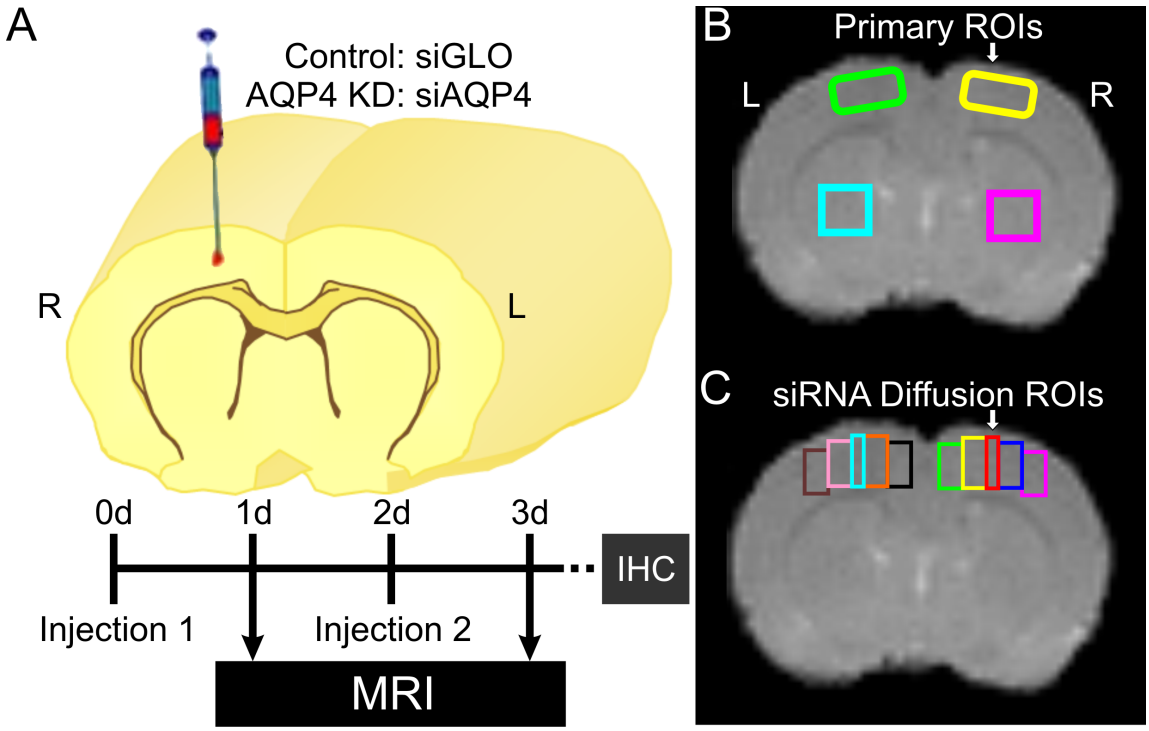

Figure 3.1: Experimental Design.

A. siAQP4 or siGLO was injected 1 mm below the cortical surface in the left (R) parietal cortex (4 µl at 0.5 µl/min) using a Hamilton syringe at 0 and 2 days in P17 rat pups. MRI was performed at 1 and 3 days and pups were perfused for immunohistochemical (IHC) analysis after the last MRI scan. B. Regions of interest (ROIs) were delineated on T2-weighted images (T2WI) and overlaid onto T2 and apparent diffusion coefficient (ADC) maps. The primary ROIs included 4 regions (ipsi- and contralateral cortex and striatum) to evaluate siAQP4 efficacy at the injection site (arrow). C. To evaluate the diffusion of siRNA from the injection site (arrow), ROIs were drawn to span the entire cortex with a width of 3 pixels at the injection site and 2 ROIs medial and lateral from the injection with a width of 5 pixels. Abbreviations: KD = knockdown, L = left hemisphere.

The 4 μL of mixture of either siAQP4 or siGLO was injected into the cortex at 0.5 μL/min, with a second injection repeated 2 days later (Fig 3.1A). For regional and cellular distribution of siRNA in the brain, a single injection of non-targeted siRNA (siGLO) tagged with the fluorescent dye, DY-5473, was used 3 days after the initial siRNA injection. Rat brains were freshly collected (n=4) and frozen for protein analysis and other rats (n=7) were transcardially perfused with 4% paraformaldehyde for immunohistochemistry.

Magnetic Resonance Imaging Experiments and Analysis. MRI was performed at 3 days after siRNA and siGLO injection (n=4, per group). Rats were lightly anesthetized using isoflurane (1.0%) and then imaged on a Bruker Avance 11.7 T MRI (Bruker Biospin, Billerica, MA, USA) (Badaut et al., 2007, Obenaus et al., 2007). Two imaging data sets were acquired: (1) a 10 echo T2 and (2) a diffusion weighted sequence, where each sequence collected 20 coronal slices (1 mm thickness and interleaved by 1 mm). The T2 sequence had the following parameters: TR/TE (time to repetition/echo time) = 4,600 ms / 10.2 ms, matrix = 128 x 128, field of view = 3 cm, NEX (number of acquisitions) = 2 and acquisition time = 20 minutes. The spin echo diffusion sequence parameters were TR/TE = 3,000 ms / 25 ms, b values = 0.72, 1,855.64 s/mm^2, matrix = 128 x 128, field of view = 3 cm, NEX = 2, and acquisition time = 25 minutes.

T2 and ADC values were quantified using standardized protocols published previously (Badaut et al., 2007, Obenaus et al., 2007) on a single coronal slice (1 mm thick) at the site of the injection (Fig 3.1B) and at the same

level used for histology analysis. T2 maps were generated and ADC maps were calculated using a linear two-point fit. Four primary regions of interest (ROIs) within ipsi- and contralateral hemispheres (cortex and striatum) were delineated on T2-weighted images (T2WI) (Fig 3.1B). These ROIs were overlaid onto corresponding T2 and ADC maps and the mean, standard deviation, number of pixels and area for each ROI were extracted. MRI analysis was performed by two blinded readers without knowledge of treatment. The intraobserver variability was found to be 2% in siGLO-treated pups and 7% in the siAQP4-treated pups.

For a more detailed analysis of the spatial and temporal distribution of siRNA in the brain, rat pups with a single injection of siGLO were used. siRNA diffusion ROIs were drawn on T2 images and transferred onto T2 and ADC maps (Fig. 3.1C). Regions spanned the entire cortex with a width of 3 pixels at the injection site and 2 regions medial and lateral from the injection site with a width of pixels. These were then copied to the contralateral cortex.

Western Blot Analysis. After imaging, four animals were freshly dissected and seven were transcardially perfused with 4% paraformaldehyde. The freshly dissected brains were frozen and cut at -20^{o}C on a cryostat (Leica, Glattbrugg, Switzerland). Quantification of AQP4 Western blots was performed as previously described (Hirt et al., 2009). Protein was prepared from tissue slices obtained from frozen brains of siGLO- and siAQP4-treated rat pups. Slices were prepared in an appropriate buffer (Hirt et al., 2009) and sonicated for 30 seconds. A measure of 1 mg of protein was then subjected to SDS

polyacrylamide gel electrophoresis on a 12% gel (Nupage, Invitrogen, Carlsbad, CA) for the quantification of AQP4. Proteins were then transferred to a polyvinylidene fluoride membrane (PerkinElmer, Schwerzenbach, Switzerland). The blot was incubated with a polyclonal antibody against AQP4 (Chemicon, Temecula, CA, 1:3,000) and a monoclonal antibody against actin (Sigma, Buchs, Switzerland, 1:25,000) in Odyssey blocking buffer (LI-COR Biosciences, Lincoln, NE) overnight at 41^{o}C. After washing, the filter was incubated with two fluorescence-coupled secondary antibodies (1:10,000, anti-rabbit Alexa Fluor 680 nm, Molecular Probes, Eugene, OR and anti-mouse immunoreactivity (IR)-Dye-800 nm, Roche, Basel, Switzerland) for 2 hours at room temperature. After washing, the degree of fluorescence was measured using an infrared scanner (Odyssey, LI-COR Bioscience, Lincoln, NE). Quantification was performed blindly by two experimenters for total AQP4 (Hirt et al., 2009).

Immunohistochemistry and Image Analysis. The fixed brains were put in 30% sucrose in phosphate buffered saline (PBS) solution for cryoprotection before freezing and cutting on a cryostat.

IgG staining for blood–brain barrier evaluation: Sections were incubated for 4 hours at room temperature with biotin-conjugated affinity purified donkey anti-rat immunoglobulin G (IgG) coupled with biotin (Vector Laboratories, Burlingame, CA, 1:200) and then a streptavydin-coupled IR-dye-680nm (Molecular Probes) diluted (1:400) in PBS containing 0.1% Triton X-100 and 1% bovine serum albumin. After washing, sections were scanned on an Odyssey

infrared scanner to quantify fluorescence using the same ROIs as defined in MRI experiments on two adjacent slices. The IR was quantified and fluorescence was converted into average integrated intensities from the ipsilateral and contralateral hemispheres. The integrated intensities were expressed as a percent of values from control rats.

AQP4/GFAP/NeuN immunohistochemistry: Commercially available, affinity purified, rabbit polyclonal antibodies were used for AQP4 and glial fibrillary acidic protein (GFAP) immunolabeling (Chemicon International, Temecula, CA), and mouse monoclonal antibodies were used for GFAP and neuronal nuclei (NeuN, Chemicon International, Temecula, CA) labeling. Immunostaining was performed in PBS containing 0.1% Triton X-100 and 0.3% bovine serum albumin and after each incubation, sections were rinsed in PBS 3 x 10 minutes.

For immunolabeling, sections were first incubated overnight at 4^{o}C with anti-AQP4 (1:300), GFAP (1:400), and NeuN (1:500). After washing, floating sections were incubated for 2 hours at room temperature with secondary antibodies.

IR immunofluorescence was performed for AQP4 and GFAP staining using secondary antibodies containing an IR-dye-680-nm secondary anti-rabbit (1:1,000, Molecular Probes, Eugene, OR) and an IR-dye-800-nm secondary anti-rabbit (1:1,000, Roche, Basel, Switzerland) antibody. Sections were scanned with an Odyssey IR scanner and fluorescence was quantified (Badaut et al.,

2007). The fluorescence from AQP4-IR and GFAP-IR were quantified with four ROIs placed in ipsilateral and contralateral cortices and striatum.

In a second set of experiments, Alexa-Fluor-594nm coupled secondary rabbit antibody (Molecular Probes, Invitrogen, 1:500) and Alexa-Fluor-468nm coupled secondary mouse antibody (Molecular Probes, Invitrogen, 1:500) were used to reveal anti-AQP4, anti-GFAP, and anti-NeuN. Sections were mounted and coverslipped with anti-fading medium Vectashield containing DAPI (Blue color in pictures, Vector, Vector Laboratories). Immunofluorescent preparations were examined using confocal laser scanning microscopy (Zeiss, Feldbach, Switzerland) and epifluorescence microscopy (Olympus, BX41, Switzerland). Optical density measurements of AQP4 immunoreactivity was performed using Morpho-Expert (Explora-Nova, La Rochelle, France) on 1 mm thick confocal laser scanning microscopy images at three different levels in each slice and in three different regions of the ipsilateral and contralateral cortex and striatum. All measurements were performed by two blinded experimenters on raw images from four independent series of immunohistochemical experiments. This method of quantification showed the same trends observed with IR immunohistochemistry.

NeuN-positive cells were counted in the four selected ROIs each one containing 80 to 95 different fields (422 x 338 μm^2). The counting of NeuN-positive nuclei was automatically performed using Mercartor software (Explora-Nova). The accuracy of the counting was previously tested on slices from control

rats stained with NeuN and DAPI, and no significant differences were observed between the two hemispheres.

For astrocyte morphology, convexity factors were measured using Morpho-Expert (Explora-Nova) from GFAP stained tissues. This factor was calculated using the following: convexity factor = Ph/Pc, where Ph and Pc are the perimeters of the convex hull and cell, respectively (Soltys et al., 2005). These values were semiautomatically calculated from binarized images from three different areas inside the ipsilateral and contralateral cortex and striatum in four independent series of immunohistochemistry experiments, using Morpho-expert (Explora-Nova).

For all immunohistochemical experiments, controls were performed by omitting the primary antibody, which gave negative results with no detectable labeling. Depletion of the AQP4 antibody by an excess of the specific peptide (Chemicon International) was also performed and gave negative results as previously observed (de Castro Ribeiro et al., 2006).

Statistical Analysis. All data are presented as the mean ± SEM and statistical analysis was performed using GraphPad InStat version 3.05 (GraphPad Software, San Diego, CA, USA) and (Sigmastat, SPSS Inc., Chicago, IL, USA). A Kolmogorov and Smirnov test was first performed to assess the Gaussian distribution of the data. Data that passed the test were analyzed with an unpaired t-test, and analysis of variance followed by Tukey–Kramer multiple

comparison tests. For Western blot analysis, the nonparametric Wilcoxon and Kruskal–Wallis test was used.

Results

In Vivo Small Interfering RNA Diffusion and Cell Transfection. Injection of siGLO tagged with DY-547, a fluorescent dye, showed diffusion of siRNA along the corpus callosum, into the contralateral cortex and bilaterally into the striatum (Fig 3.2A, B). Astrocytes were positively transfected by siAQP4 as demonstrated by the presence of DY-547 fluorescence in GFAP-positive cells (Fig 3.2B). This protocol allowed us to study siAQP4 effects on brain areas remote from the injection site including the contralateral striatum (Fig. 3.2B3).

AQP4 Expression After Small Interfering RNA Against AQP4. Western blot analysis of the ipsilateral brain hemisphere showed that AQP4 expression was decreased by 27% in siAQP4-treated rat pups compared with controls (1.23 ± 0.11 in control versus 0.90 ± 0.09 in siAQP4, $p < 0.05$, Fig. 3.3A, B).

Immunohistochemistry demonstrated that perivascular AQP4 expression was decreased in the ipsilateral cortex adjacent to the site of injection (Fig. 3.3C1, C2, E). In the contralateral striatum (Fig. 3.3D), AQP4 staining was also significantly decreased compared with siGLO (11.4 ± 1.9 versus 18.6 ± 1.5, $p < 0.01$, Fig. 3.3D1, D2, and E). A decrease in AQP4 staining was observed on the astrocyte endfeet in contact with blood vessels, in the neuropil and in the glia

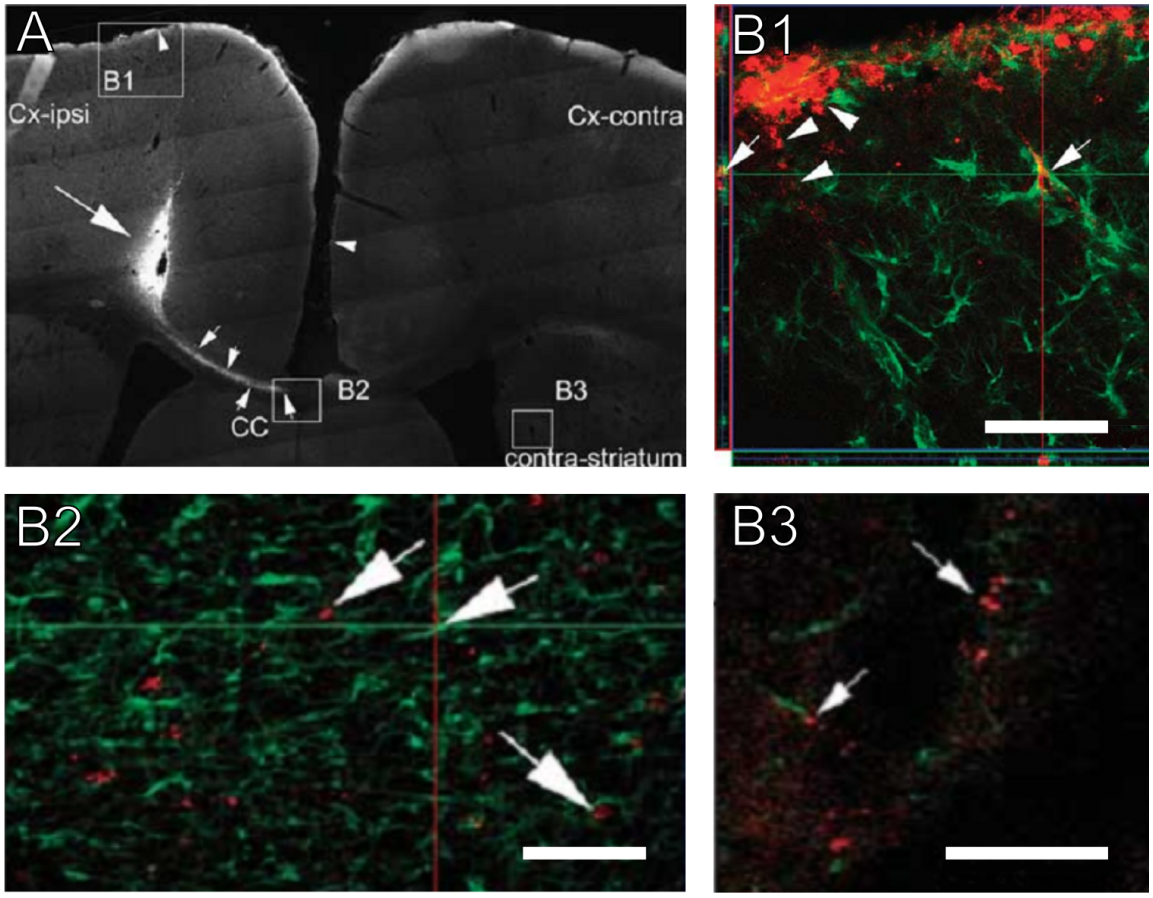

Figure 3.2: siAQP4 Diffuses within Brain Tissues.

A. Diffusion of siGLO tagged with DY-547 in a rat coronal section at the site of injection. siRNA was observed in the cortex (cx) at the site of injection (large arrow) and diffused within the brain parenchyma towards the contralateral striatum via the corpus callosum (CC, small arrows). B. Confocal images of GFAP (green) and siGLO-DY547 (red) immunostaining at 3 days after the initial injection in the ipsilateral cortex (B1), CC (B2), and contralateral striatum (B3). Double staining revealed positive DY-547 in astrocytes (B1, arrows) around blood vessels and also in the glia limitans (arrowheads) in close proximity to the injection site. Several astrocytes were transfected by the tagged siRNA. In the CC (B2), siRNA was detected in astrocytes (arrows), showing that siRNA is able to diffuse via the CC to the contralateral hemisphere. Far from the injection site (B3), siGLO-DY547 was observed in astrocytes in contact with blood vessels within the contralateral striatum. Scale bar = 50 μm. (Images provided by J. Badaut)

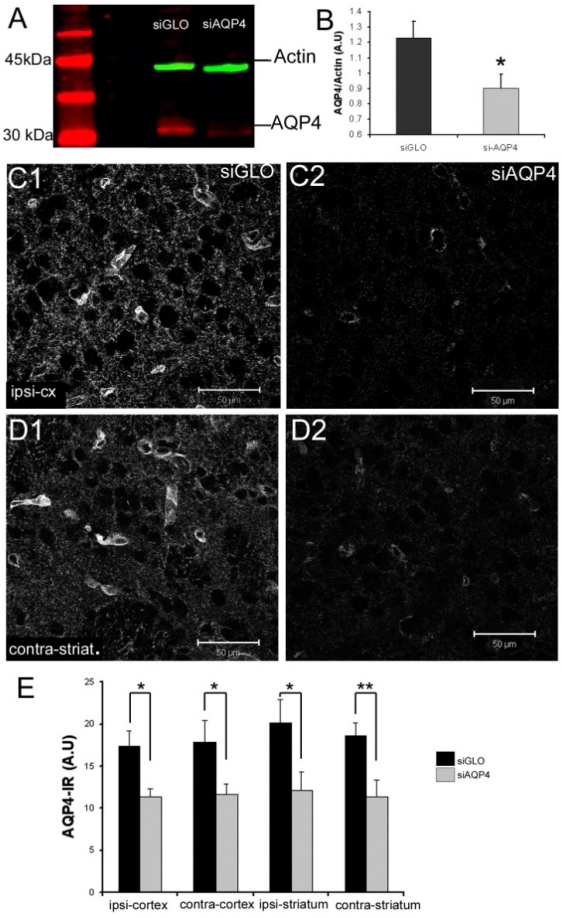

Figure 3.3: Efficiency of AQP4 Inhibition with siRNA.

A. AQP4 expression in siGLO- and siAQP4-treated rat pups was analyzed by Western blot. A 30 kDa band was observed (red) in siGLO pups. The intensity of the signal was decreased in siAQP4-treated rats, with no change in the intensity of the actin band (green). B. Expression of AQP4 was decreased (0.9 ± 0.09 arbitrary units, A.U.) in siAQP4 compared with siGLO animals (1.22 ± 0.11 A.U., *p < 0.05). C. AQP4 immunolabeling was also performed to examine variations in AQP4 expression in situ. C. Confocal images of AQP4 staining in siGLO (C1) and siAQP4 (C2) rat pups showed a significant decrease in the intensity of AQP4 staining in the ipsilateral cortex of siAQP4 rats. D. AQP4 labeling in the contralateral striatum of the siGLO- (D1) and siAQP4-treated rat pups (D2) also revealed decreased AQP4 expression, consistent with our Western blot analysis. E. AQP4 immunolabeling was quantified using optical densitometry demonstrating a decrease in all brain areas (*p < 0.05). (Figure provided by J. Badaut)

limitans (Fig 3.3C-D). Interestingly, the level of AQP4 expression in cells lining the third ventricle was not changed.

Morphological Tissue Analysis. Several histological and morphological analyses were undertaken to demonstrate that decreased AQP4 levels were not due to altered tissue composition. In the ipsilateral cortex close to the needle track, there was no significant difference in the number of neurons in siAQP4-treated (1,139 ± 30 per mm^2) compared with siGLO-treated rat pups (998 ± 62 per mm^2, Fig 3.4A, B), suggesting that silencing AQP4 is not toxic to neurons. In the ipsilateral cortex, GFAP staining revealed that gliosis formation due to insertion of the needle was reduced 58.3% in siAQP4-treated rat pups compared with siGLO controls ($p < 0.05$, Fig. 3.5A1, A2, and C). Increased IgG staining in the ipsilateral cortex of siGLO-treated pups was consistent with needle track induced blood–brain barrier (BBB) disruption, but increased IgG staining was not observed in siAQP4-treated pups (Fig. 3.4C). These results suggest that BBB disruption was minimized in the siAQP4-treated animals at the site of the injection compared with siGLO-treated rats (Fig. 3.4C), a finding that correlates well with our observed lack of gliosis (Fig. 3.5A1, A2, and C).

One important observation was that AQP4 expression was decreased at sites distant from the site of injection (ipsilateral striatum and contralateral cortex and striatum, Fig. 4). In the contralateral striatum, the neuronal count showed no difference between siAQP4- (1,145 ± 38 per mm^2) and siGLO-treated rats (1,229 ± 53 per mm^2) (Fig 3.4B). Astrocytic GFAP expression was also not significantly

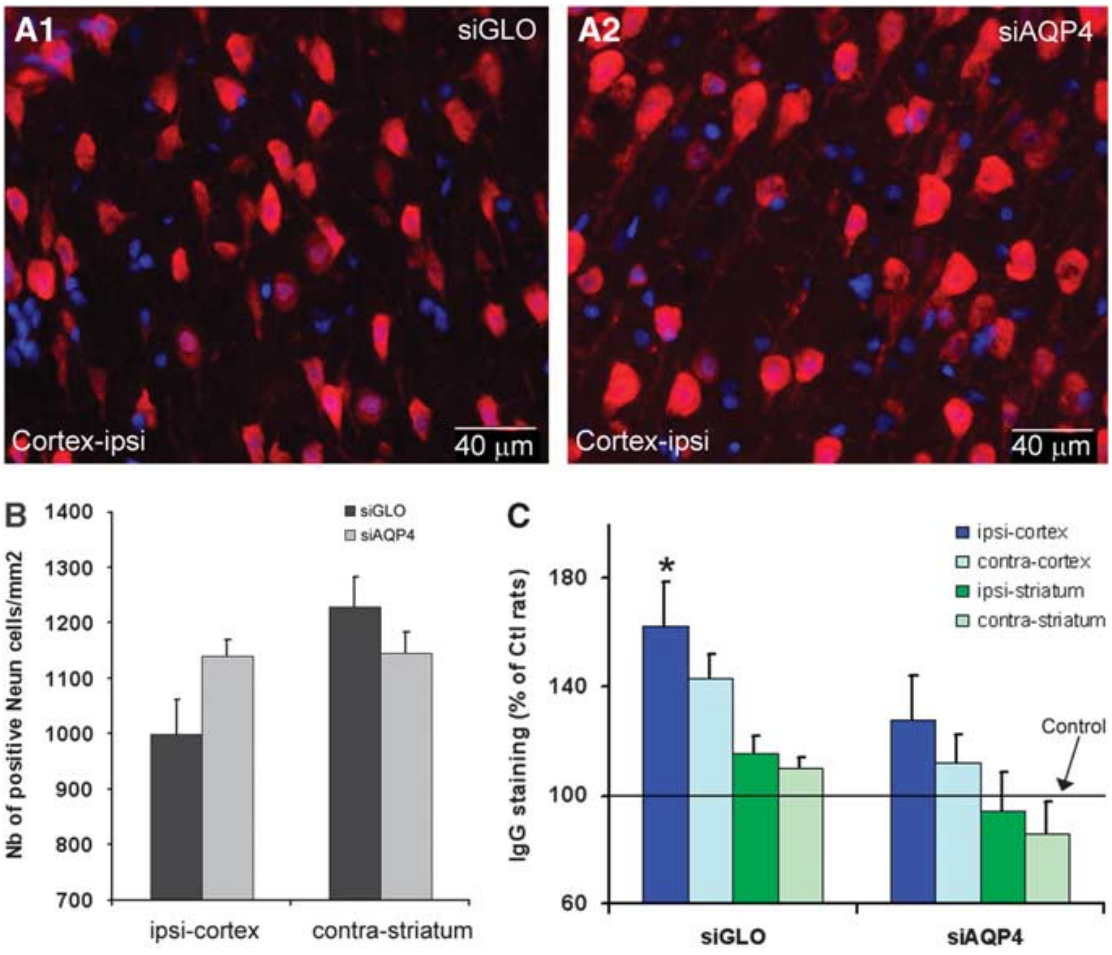

Figure 3.4: Effects of siAQP4 Injection on Neuronal Survival and Blood–Brain Barrier (BBB) integrity

A. Neuronal changes were evaluated using NeuN (red) immunolabeling and counterstained with DAPI staining for cell nuclei (blue) in the ipsilateral cortex (cortex-ipsi) of siGLO- (A1) and siAQP4-treated (A2) rats. B. The number of NeuN positive cells in 4 different regions of interest was not significantly altered in the siAQP4-treated compared with the siGLO-treated rats. In ipsi-cortex, the number of neurons in siAQP4-treated pups was higher than in the siGLO rats. Similarly, no significant results were seen in the contralateral striatum of siAQP4-treated versus siGLO-treated pups. C. IgG staining was used to evaluate blood-brain barrier (BBB) integrity 3 days after siGLO and siAQP4 injection in four ROIs (ipsilateral and contralateral cortex and striatum). In siGLO-treated rats, IgG staining was increased within the ipsilateral cortex (*$p < 0.05$) compared with controls and siAQP4-treated pups. In the other ROIs, there were no significant modifications of IgG staining compared with control values suggesting that the BBB was not affected. (Figure provided by J. Badaut)

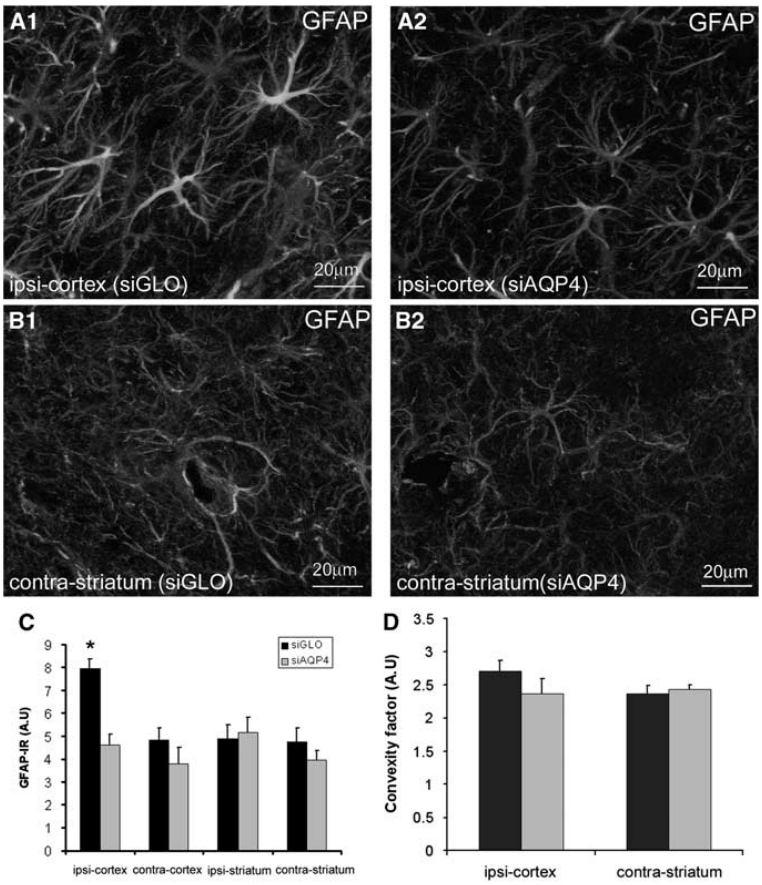

Figure 3.5: siAQP4 has no Effect on Astrocyte Morphology.

A-B. Astrocyte morphology using GFAP staining was examined in siGLO- (A1, B1) and in siAQP4-treated rat pups (A2, B2) in the ipsilateral cortex (ipsi-cortex) adjacent to the injection site (A) and in the contralateral striatum (contra-striatum, B). There was increased GFAP staining intensity in siGLO-treated (A1) compared with siAQP4-treated rats (A2) in the ipsi-cortex. In the contra-striatum, GFAP staining in siGLO pups (B1) and in siAQP4-treated rats (B2) showed no differences in staining intensity. The presence of siAQP4 did not significantly affect the morphology of the astrocytes in the ipsi-cortex or contra-striatum. C. Quantification of GFAP immunoreactivity (IR) showed a significant increase in the ipsi-cortex of the siGLO-treated rats (7.95 ± 0.40 A.U.) compared with the siAQP4-treated rats (4.63 ± 0.43 A.U., *$p < 0.05$) demonstrating that siAQP4 prevents an increase in GFAP expression. D. Astrocyte morphology was quantified using a convexity factor analysis and demonstrated that the presence of siAQP4 did not affect astrocyte morphology. (Figure provided by J. Badaut)

altered in the contralateral striatum in siAQP4 rats compared with siGLO (Fig 3.5B-D). Similarly, astrocyte morphology showed no difference between the groups (Fig 3.5A–D). Together, these results demonstrate that AQP4 silencing did not affect astrocyte morphology.

Reduced AQP4 Expression Elicits Decreased ADC Values. Acute AQP4 silencing resulted in a significant decrease in ADC values bilaterally within the cortex and striatum, and at distance from the site of injection in an anterior to posterior direction (Fig. 3.6). In the ipsilateral cortex at the site of injection, ADC values were decreased 33% after siAQP4 (60.8 ± 2.5 $x10^{-5}mm^2/s$) compared with siGLO-treated controls (91.1 ± 2.5 $x10^{-5}mm^2/s$, $p < 0.05$) (Fig. 3.6A, C). Decreased ADC values were also observed in the ipsilateral striatum (51%) and contralateral cortex (51%) and contralateral striatum (50%) compared with siGLO pups. In contralateral striatum, ADC values were decreased 51% (siAQP4, 45.4 ± 1.7; siGLO, 92.1 ± 1.0 $x10^{-5}mm^2/s$, $p < 0.01$) (Fig. 3.6C). At 1 and 2 days after siAQP4 injection, the ADC values were not significantly altered and water content was also unchanged. Water content, based on T2WI, showed no changes at 3 days (Fig. 3.6B, D).

Early Reduction in ADC values surrounding siAQP4 injection. To evaluate the diffusion of siRNA in the brain tissue, we performed a single injection of either siGLO or siAQP4 into the cortex and quantified ADC values surrounding the injection site at 1 and 3 days (Fig. 3.1C). ADC values decreased surrounding the injection site in siAQP4 rat pups compared to siGLO pups at 1

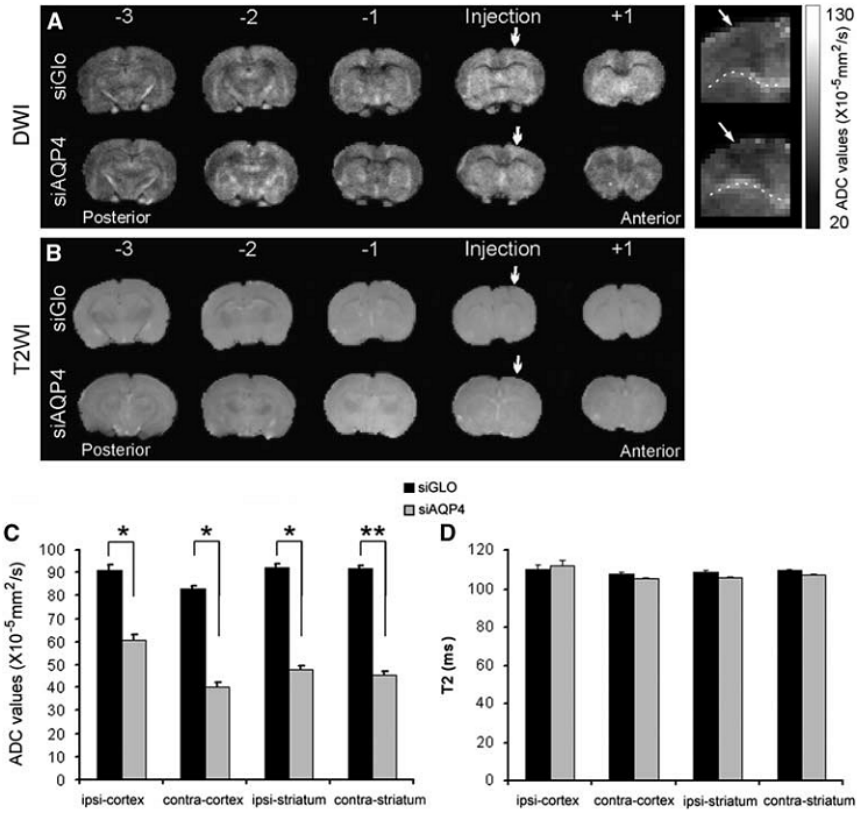

Figure 3.6: Apparent Diffusion Coefficient (ADC) and T2 Values after siAQP4 Injection.

A. *In vivo* diffusion-weighted images (DWI) for siGLO- and siAQP4-treated rat pups from anterior to posterior brain regions from the injection site (arrows). A global decrease in ADC values was observed at several levels (+1, injection site, -1, -2, -3). Enlarged ADC images focusing on the contralateral cortex (contra-cortex) showed a decrease in ADC in siAQP4 compared with siGLO rats (right panel). Arrows illustrate decreased ADC location in the cortex (dotted line indicates corpus callosum). The quantification of the ADC was performed at the site of injection at the same level used for the histology. B. The *in vivo* T2 was recorded from siGLO- and siAQP4-treated pups from anterior to posterior brain regions from the injection site (arrows). No changes were observed within the brains of both groups. C. In the ipsilateral cortex (ipsi-cortex), ADC values in siAQP4-treated rats were significantly decreased to 60.8 ± 2.5 compared with 91.1 ± 2.5 ($x10^{-5}$ mm^2/s) in siGLO rats representing a 33% reduction (*$p < 0.05$). Similarly, a 50% decrease was observed in ipsilateral striatum and in contralateral cortex and striatum. In the contralateral striatum, ADC values were 45.4 ± 1.7 in siAQP4 pups compared with 92.1 ± 1.0 in siGLO representing a 51% decrease (**$p < 0.01$). D. T2 values, measured in siGLO and siAQP4 rat pups were not significantly different between brain regions suggesting that brain water content was not changed.

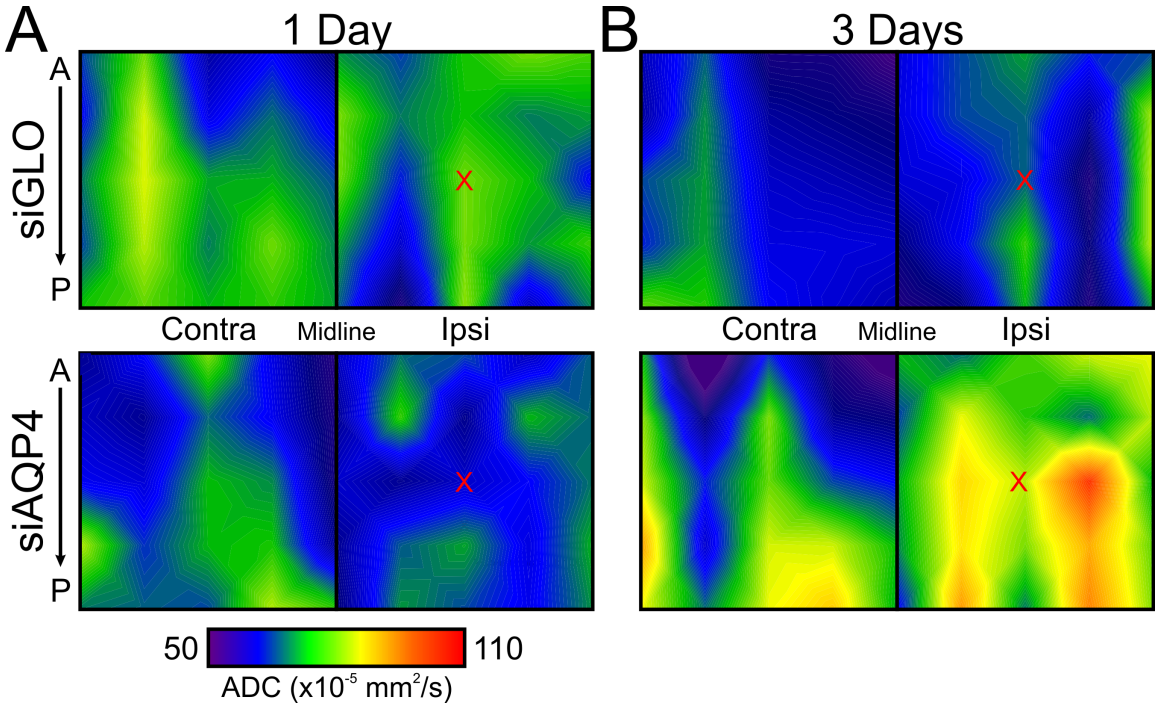

Figure 3.7: siRNA Diffusion from the Injection Site after a Single Injection.

A. Apparent diffusion coefficient (ADC) values were calculated in siGLO and siAQP4 rats surrounding the injection site (red X). siRNA diffusion regions of interest (see Fig. 3.1C) were placed in the ipsilateral (ipsi) and contralateral (contra) cortices and then copied to 2 slices anterior (A) and posterior (P) from the injection site. At 1 day, a decrease in ADC values was observed at the injection site after siAQP4 injection, which extended from anterior to posterior and into the contralateral hemisphere. B. At 3 days, elevated ADC values were observed in the siAQP4 group in the ipsilateral cortex compared to the siGLO group.

day (Fig. 3.7A). Interestingly, this decrease in ADC was also seen on the contralateral cortex, consistent with our histological observation of siRNA in the contralateral hemisphere (corpus callosum and striatum) (Fig. 3.3D2). At 3 days, ADC values in the siAQP4 group rebound above ADC values within siGLO ipsilateral hemisphere (Fig. 3.7B). These data suggest that a single injection of siAQP4 is insufficient to decrease water mobility beyond 3 days in rats, thus multiple injections are necessary.

Discussion

The principal novel finding of the current study is that silencing AQP4 expression resulted in a decrease in water mobility, as measured using MRI-derived ADC values in normal brain tissue. Our results strongly suggest that astrocytes, and in particular their water channels, greatly contribute to water mobility.

Until now, the contribution of brain AQP4 to water movement has primarily been shown in astrocyte cultures prepared from wild-type mice treated with siRNA or from AQP4-knockout ($AQP4^{-/-}$) mice (Nicchia et al., 2003, Manley et al., 2004, Nicchia et al., 2005). *In vivo*, the role of AQP4 in water movement was evaluated in several pathological models using transgenic mice (Manley et al., 2004). AQP4 was shown to have a key but dual role in edema formation and resolution (Tait et al., 2008). Using transgenic mice lacking AQP4 ($AQP4^{-/-}$), the authors showed that AQP4 aggravated cytotoxic edema formation (Manley et al.,

2000) and likewise facilitated water removal in vasogenic edema (Papadopoulos et al., 2004). Alternative existing mouse models have also been used to study the role of AQP4, including the dystrophin null mdx-b transgenic mouse (mdx) and the α-syntrophin null mouse ($Syn^{-/-}$) (Vajda et al., 2002, Amiry-Moghaddam et al., 2003, Nico et al., 2003). These transgenic mice have normal AQP4 protein levels but a significant reduction in AQP4 expression in the astrocytic foot processes surrounding blood vessels and at the glia limitans (Vajda et al., 2002, Amiry-Moghaddam et al., 2003, Nico et al., 2003). These previous experiments have confirmed that AQP4 has an important role in cytotoxic edema formation in water intoxication and stroke models (Vajda et al., 2002, Amiry-Moghaddam et al., 2003, Nico et al., 2003).

Under normal physiological conditions, Manley and colleagues (2004) reported that brains from wild-type and $AQP4^{-/-}$ mice did not reveal gross anatomical differences by light microscopy and structural MRI. However, the extracellular space was increased in the $AQP4^{-/-}$ compared with wild-type mice (Binder et al., 2004, Yao et al., 2008). Despite the increase of the extracellular space, the diffusional properties for large molecules was not different between these $AQP4^{-/-}$ and wild-type mice (Xiao and Hrabetova, 2009). The mdx and $Syn^{-/-}$ mice display baseline morphological abnormalities, including swollen astrocyte foot processes (Amiry-Moghaddam et al., 2004) and increased BBB permeability (Frigeri et al., 2001, Nico et al., 2003). However, these abnormalities did not alter MRI measurements in mdx mice, where brain ADC values were similar between

mdx and wild-type mice (Vajda et al., 2002). In these murine models, deletion of dystrophin and syntrophin may affect other transporters and proteins with potential compensatory mechanisms inhibiting any observable changes in ADC values.

Until now, the contribution of astrocytic AQP4 in water diffusion has never been investigated directly *in vivo* in normal brain. *In vitro*, the water permeability of cells has been indirectly determined by measuring the kinetics and the maximum degree of astrocyte cell swelling in response to solution exchange between isotonic and hypotonic saline (Nicchia et al., 2003, Nicchia et al., 2005). Cell swelling is significantly reduced in astrocytes that did not express AQP4, suggesting that this water channel contributes significantly to astrocytic water movement *in vitro* (Nicchia et al., 2003, Nicchia et al., 2005). Similarly, cortical injection of siAQP4 induced a decrease in AQP4 at the site of injection and remotely in the contralateral striatum (Fig. 3.3) after 3 days. The 27% decrease in AQP4 in the ipsilateral hemisphere did not affect astrocyte morphology based on GFAP analysis (Fig. 3.5). Thus, at 3 days, decreased AQP4 levels induced a significant decrease in ADC values without modification of tissue histology, BBB disruption, neuronal cell death or significant modification of astrocyte morphology (Fig. 3.4-5). Evaluation of ADC before 3 days did not reveal any decrements, consistent with the notion that a threshold reduction in AQP4 expression is needed to elicit the 50% reduction in ADC values reported in our studies.

Furthermore, serial evaluation of siRNA diffusion has never been investigated. *In vivo* diffusion analysis of quantum dots and growth factors in the extracellular space of the rat brain has helped establish size limits for therapeutic agents (Thorne et al., 2004, Thorne and Nicholson, 2006). The extracellular space can range from 20 to 40 nm and decrease to as little as 10 nm after ischemia (Thorne and Nicholson, 2006). Although the average size of a single siRNA is below 10 nm, reaching the limit of the extracellular space width can significantly affect its diffusion through the parenchyma (Guo et al., 2010). In the normal brain, ADC values decreased in the ipsilateral cortex after a single injection siAQP4 (Fig. 3.7). Surprisingly, the contralateral cortex also had decreased ADC values compared to a single siGLO injection. This decrease was transient and at 3 days, ADC values quickly rose in siAQP4 pups and surpassed ADC values in siGLO pups. This increase in ADC at 3 days could be due to a compensatory mechanism in response to the earlier down regulation of AQP4, but is currently unknown and should be examined further. Determining siRNA *in vivo* properties such as diffusion and its transient inhibition will help improve siRNA-based therapeutics to down-regulate expression in a spatially- and temporally-controlled fashion (i.e. number of injection and distance between injections).

Together, our results in the normal brain revealed that AQP4 significantly contributes to ADC values, a measure of water diffusion. Previously, decreased ADC values have been related to a decrease in the extracellular space as a

consequence of cellular swelling under pathological conditions. Early decreases in ADC values in the hypoxic-ischemic rat model correlated with decreased AQP4 expression (Meng et al., 2004). In a rat model of hydrocephalus, an increased level of AQP4 expression correlated with increased ADC (Tourdias et al., 2009). Previous work in pathological conditions and our study in normal brain suggest that altered astrocyte water permeability likely has a critical role in water mobility. The contribution of astrocytic AQP4 to ADC values reinforces the importance of the astrocytic compartment in neuroimaging.

The needle induced a mild mechanical lesion with an increase in GFAP staining in the ipsilateral cortex and BBB disruption (Fig. 3.4-5). Interestingly, we observed that siAQP4 injection prevented the increase in GFAP and BBB disruption induced by the needle track (Fig. 3.4-5). These observations suggest that injection of siAQP4 may prevent gliosis formation and BBB disruption induced by mechanical forces. Our results are in accordance with previous reports in $AQP4^{-/-}$ mice showing that the absence of AQP4 protects against cell death caused by edema (Manley et al., 2000, Saadoun et al., 2009) and inhibits glial scar formation (Saadoun et al., 2005, Auguste et al., 2007). Our results suggest a promising future for the use of siRNA therapies against AQP4. We speculate that this novel approach of AQP4 silencing could be used to prevent edema formation after acute brain injury, particularly with improved methods of drug delivery (e.g. intranasal route).

The cellular location of AQP4 in astrocytic endfeet in contact with cerebral blood vessels suggests a role in BBB modulation (Wolburg et al., 2009). $AQP4^{-/-}$ mice showed both disruption (Zhou et al., 2008) and no change of the BBB (Saadoun et al., 2009). In our experience, decreased AQP4 at sites distant from the injection site (contralateral striatum) did not alter BBB permeability (Fig. 3.4C). In accordance with previous studies, our results demonstrate that decreased AQP4 does not induce leakage of the BBB (Saadoun et al., 2009). Our results are consistent with the idea that AQP4 is not critical for BBB maintenance in normal brain, in the absence of mechanical or metabolic stress.

In conclusion, involvement of AQP4 in modulating ADC values strengthens the role of the neurovascular unit in regulating water movement under normal and pathological conditions, where decreased ADC values are usually interpreted as reflective of cytotoxic edema, which may be due to decreased AQP4 expression. The contribution of astrocytic AQP4 to ADC values reinforces the importance of the astrocytic compartment in neuroimaging.

Chapter 3 References

Amiry-Moghaddam M, Otsuka T, Hurn PD, Traystman RJ, Haug FM, Froehner SC, Adams ME, Neely JD, Agre P, Ottersen OP, Bhardwaj A (2003) An alpha-syntrophin-dependent pool of AQP4 in astroglial end-feet confers bidirectional water flow between blood and brain. Proc Natl Acad Sci U S A 100:2106-2111.

Amiry-Moghaddam M, Xue R, Haug FM, Neely JD, Bhardwaj A, Agre P, Adams ME, Froehner SC, Mori S, Ottersen OP (2004) Alpha-syntrophin deletion removes the perivascular but not endothelial pool of aquaporin-4 at the blood-brain barrier and delays the development of brain edema in an experimental model of acute hyponatremia. FASEB J 18:542-544.

Auguste KI, Jin S, Uchida K, Yan D, Manley GT, Papadopoulos MC, Verkman AS (2007) Greatly impaired migration of implanted aquaporin-4-deficient astroglial cells in mouse brain toward a site of injury. FASEB J 21:108-116.

Badaut J, Ashwal S, Tone B, Regli L, Tian HR, Obenaus A (2007) Temporal and regional evolution of aquaporin-4 expression and magnetic resonance imaging in a rat pup model of neonatal stroke. Pediatr Res 62:248-254.

Badaut J, Lasbennes F, Magistretti PJ, Regli L (2002) Aquaporins in brain: distribution, physiology, and pathophysiology. J Cereb Blood Flow Metab 22:367-378.

Binder DK, Papadopoulos MC, Haggie PM, Verkman AS (2004) In vivo measurement of brain extracellular space diffusion by cortical surface photobleaching. J Neurosci 24:8049-8056.

de Castro Ribeiro M, Hirt L, Bogousslavsky J, Regli L, Badaut J (2006) Time course of aquaporin expression after transient focal cerebral ischemia in mice. J Neurosci Res 83:1231-1240.

Frigeri A, Nicchia GP, Nico B, Quondamatteo F, Herken R, Roncali L, Svelto M (2001) Aquaporin-4 deficiency in skeletal muscle and brain of dystrophic mdx mice. FASEB J 15:90-98.

Fukuda AM, Adami A, Pop V, Bellone JA, Coats JS, Hartman RE, Ashwal S, Obenaus A, Badaut J (2013) Posttraumatic reduction of edema with aquaporin-4 RNA interference improves acute and chronic functional recovery. J Cereb Blood Flow Metab, doi:10.1038/jcbfm.2013.118.

Guo P, Coban O, Snead NM, Trebley J, Hoeprich S, Guo S, Shu Y (2010) Engineering RNA for targeted siRNA delivery and medical application. Advanced Drug Delivery Reviews 62:650-666.

Hirt L, Ternon B, Price M, Mastour N, Brunet J-F, Badaut J (2009) Protective role of early Aquaporin 4 induction against postischemic edema formation. Journal of Cerebral Blood Flow & Metabolism 29:423-433.

Le Bihan D (2003) Looking into the functional architecture of the brain with diffusion MRI. Nat Rev Neurosci 4:469-480.

Manley GT, Binder DK, Papadopoulos MC, Verkman AS (2004) New insights into water transport and edema in the central nervous system from phenotype analysis of aquaporin-4 null mice. Neuroscience 129:983-991.

Manley GT, Fujimura M, Ma T, Noshita N, Filiz F, Bollen AW, Chan P, Verkman AS (2000) Aquaporin-4 deletion in mice reduces brain edema after acute water intoxication and ischemic stroke. Nat Med 6:159-163.

Meng S, Qiao M, Lin L, Del Bigio MR, Tomanek B, Tuor UI (2004) Correspondence of AQP4 expression and hypoxic-ischaemic brain oedema monitored by magnetic resonance imaging in the immature and juvenile rat. The European Journal of Neuroscience 19:2261-2269.

Nicchia GP, Frigeri A, Liuzzi GM, Svelto M (2003) Inhibition of aquaporin-4 expression in astrocytes by RNAi determines alteration in cell morphology, growth, and water transport and induces changes in ischemia-related genes. FASEB J 17:1508-1510.

Nicchia GP, Srinivas M, Li W, Brosnan CF, Frigeri A, Spray DC (2005) New possible roles for aquaporin-4 in astrocytes: cell cytoskeleton and functional relationship with connexin43. FASEB J 19:1674-1676.

Nico B, Frigeri A, Nicchia GP, Corsi P, Ribatti D, Quondamatteo F, Herken R, Girolamo F, Marzullo A, Svelto M, Roncali L (2003) Severe alterations of endothelial and glial cells in the blood-brain barrier of dystrophic mdx mice. Glia 42:235-251.

Obenaus A, Ashwal S (2008) Magnetic resonance imaging in cerebral ischemia: focus on neonates. Neuropharmacology 55:271-280.

Obenaus A, Robbins M, Blanco G, Galloway NR, Snissarenko E, Gillard E, Lee S, Curras-Collazo M (2007) Multi-modal magnetic resonance imaging alterations in two rat models of mild neurotrauma. J Neurotrauma 24:1147-1160.

Papadopoulos MC, Manley GT, Krishna S, Verkman AS (2004) Aquaporin-4 facilitates reabsorption of excess fluid in vasogenic brain edema. FASEB J 18:1291-1293.

Saadoun S, Papadopoulos MC, Watanabe H, Yan D, Manley GT, Verkman AS (2005) Involvement of aquaporin-4 in astroglial cell migration and glial scar formation. Journal of Cell Science 118:5691-5698.

Saadoun S, Tait MJ, Reza A, Davies DC, Bell BA, Verkman AS, Papadopoulos MC (2009) AQP4 gene deletion in mice does not alter blood-brain barrier integrity or brain morphology. Neuroscience 161:764-772.

Soltys Z, Orzylowska-Sliwinska O, Zaremba M, Orlowski D, Piechota M, Fiedorowicz A, Janeczko K, Oderfeld-Nowak B (2005) Quantitative morphological study of microglial cells in the ischemic rat brain using principal component analysis. J Neurosci Methods 146:50-60.

Tait MJ, Saadoun S, Bell BA, Papadopoulos MC (2008) Water movements in the brain: role of aquaporins. Trends in Neurosciences 31:37-43.

Thorne RG, Hrabetova S, Nicholson C (2004) Diffusion of epidermal growth factor in rat brain extracellular space measured by integrative optical imaging. Journal of Neurophysiology 92:3471-3481.

Thorne RG, Nicholson C (2006) In vivo diffusion analysis with quantum dots and dextrans predicts the width of brain extracellular space. Proc Natl Acad Sci U S A 103:5567-5572.

Tourdias T, Dragonu I, Fushimi Y, Deloire MS, Boiziau C, Brochet B, Moonen C, Petry KG, Dousset V (2009) Aquaporin 4 correlates with apparent diffusion coefficient and hydrocephalus severity in the rat brain: a combined MRI-histological study. Neuroimage 47:659-666.

Vajda Z, Pedersen M, Fuchtbauer EM, Wertz K, Stodkilde-Jorgensen H, Sulyok E, Doczi T, Neely JD, Agre P, Frokiaer J, Nielsen S (2002) Delayed onset of brain edema and mislocalization of aquaporin-4 in dystrophin-null transgenic mice. Proc Natl Acad Sci U S A 99:13131-13136.

Wolburg H, Noell S, Wolburg-Buchholz K, Mack A, Fallier-Becker P (2009) Agrin, aquaporin-4, and astrocyte polarity as an important feature of the blood-brain barrier. The Neuroscientist 15:180-193.

Xiao F, Hrabetova S (2009) Enlarged extracellular space of aquaporin-4-deficient mice does not enhance diffusion of Alexa Fluor 488 or dextran polymers. Neuroscience 161:39-45.

Yao X, Hrabetova S, Nicholson C, Manley GT (2008) Aquaporin-4-deficient mice have increased extracellular space without tortuosity change. J Neurosci 28:5460-5464.

Zhou J, Kong H, Hua X, Xiao M, Ding J, Hu G (2008) Altered blood-brain barrier integrity in adult aquaporin-4 knockout mice. Neuroreport 19:1-5.

Chapter 4

Aquaporin-4 RNA Interference Prevents Edema Formation after Juvenile Traumatic Brain Injury

Abstract

Traumatic brain injury (TBI) is common in young children and adolescents and is associated with long-term disability and mortality. The neuropathological sequelae that result from TBI are a complex cascade of events that include edema formation and brain swelling contributing to secondary ischemic injuries. Brain aquaporin-4 (AQP4) plays a key role in edema formation. Thus, development of new clinical treatments against cerebral edema after juvenile TBI (jTBI) targeting AQP4 could reduce neurologic sequelae. We hypothesized that injection of small interfering RNA (siRNA) against AQP4 (siAQP4) after jTBI would decrease edema formation and improve neurological outcomes by inhibiting AQP4 expression. siAQP4 or a non-targeted-siRNA (siGLO) was injected lateral to the trauma site after controlled cortical impact on postnatal day 17 rats. Magnetic resonance imaging (MRI), neurological testing, and immunohistochemistry were performed to assess outcomes. siAQP4 treated rat pups had decreased edema formation, decreased of blood-brain barrier (BBB) disruption, reduced astrogliosis and neuronal cell death compared to siGLO-

treated pups after TBI. siAQP4 pups showed improvements in motor function with 33% and 46% fewer foot faults than siGLO pups at 1 and 3 days after injury. The effectiveness of our treatment paradigm is due to a 30% decrease in AQP4 expression at the injection site. Administration of siAQP4 after jTBI decreased AQP4 expression on astrocytes resulting in decreased edema formation associated with improved motor functions.

Introduction

Juvenile traumatic brain injury (jTBI) is the leading cause of death and permanent disability in infancy and childhood (Gotschall et al., 1995). jTBI is commonly accompanied by an intensified inflammatory response and increased blood-brain barrier permeability, which can result in edema formation (Kochanek, 2006). At the site of injury, edema formation can be initiated within minutes (Margulies and Hicks, 2009), and contributes to cellular swelling and secondary increases in intracranial hypertension after jTBI (Kochanek et al., 2000). Clinically, the use of magnetic resonance imaging (MRI) to evaluate water diffusion after TBI in children has been correlated with cognitive deficits (Levin et al., 2008). However, the pathomechanical response to jTBI in the developing brain are not well understood, especially ones that control edema formation (Tong et al., 2002). In order to optimize intervention with novel strategies, edema formation after brain injury needs to be better understood.

Aquaporin-4 (AQP4), a water channel, is most commonly expressed on astrocytic endfeet adjacent to blood vessels in the brain (Simard et al., 2003, Verkman, 2008). It has been shown recently that AQP4 may be important in edema formation based on in vitro and in vivo studies of water diffusion in normal brain tissue (Badaut et al., 2011a). In mice lacking AQP4, Manley and colleagues have shown decreased lesion volume compared to wild types after acute water intoxication and permanent ischemia at 24 hours (Manley et al., 2000). In contrast, AQP4 is also important for water clearance when vasogenic edema is

present (Papadopoulos et al., 2004). Taken together, a transient knockdown of AQP4 may result in the best possible outcome for brain trauma patients. Here, we examined the role of AQP4 in edema formation after controlled cortical impact (CCI) injury, a highly reproducible rodent model of TBI (Brody et al., 2007). Our novel findings demonstrate that RNA interference against AQP4 reduces brain edema and improves neurological outcomes after jTBI (Fukuda et al., 2013). Therefore, these results suggest that transient silencing of AQP4 is a viable therapeutic strategy for treatment of jTBI.

Methods and Experimental Design

Experiments and care of animals were conducted according to the principles and procedures of the Guidelines for Care and Use of Experimental Animals and approved by Loma Linda University. Sprague Dawley rat pups at postnatal day 17 (P17) were housed in a temperature controlled (64-69^{o}F) animal facility on a 12-hour light/dark cycle.

siRNA Preparation. Please refer to Chapter 3 Methods (page 43)

Cortrolled Cortical Impact (CCI) Injury and siRNA Injection. Rat pups were anesthetized with isoflurane (3% induction, 1.5-2.0% maintenance) and placed in a stereotaxic apparatus (David Kopf Instrument, Tujunga, USA). Following a midline incision over the skull, a 5 mm diameter craniotomy was drilled (Fine Science Tools Inc., Foster City, CA) over the right hemisphere using a skull trephine centered at 3 mm posterior from bregma and 4 mm lateral to

midline (-3mm AP, -4mm ML). The dura was left intact and any overt bleeding was lightly rinsed with saline solution. Rat pups were subjected to controlled cortical impact (CCI) using a electromagnetic impactor (Leica, Richmond, IL) angled 20 degrees with a 2.7 mm round tip at a velocity of 6 m/s to a depth of 1.5 mm below the cortical surface. The total duration of impact was 200 ms. Immediately after impact, siRNA was injected using a 30-gauge needle on a Hamilton syringe centered at 3 mm posterior to bregma, 6 mm lateral to midline, and 1.0 mm below cortical surface. The syringe was attached to a nanoinjector (Leica, Richmond, IL) and a total volume of 4 μL of siRNA was infused at a rate of 0.5 μL/min. The wound was sutured with non-absorbable 5-0 silk sutures (Covidien, Mansfield, MA) and all pups received an intraparetneal injection of buprenorphine (0.01 mg/kg, Tyco Healthcare Group LP, Mansfield, MA) for pain relief. Pups were then placed on a warm heating pad for recovery and returned to their dams after waking from surgery. Sham operated rat pups were treated the same but did not undergo CCI. A second injection of siRNA was repeated 2 days later in all pups using the same injection protocol (Fig. 4.1A).

Magnetic Resonance Imaging (MRI). MRI was performed at 1 and 3 days after CCI. Pups were lightly anesthetized using isoflurane (1.0%) and imaged on a Bruker Avance 11.7 T (Bruker Biospin, Billerica, MA) (Ashwal et al., 2007, Obenaus et al., 2007, Recker et al., 2009). Two imaging data sets were acquired: 1) a 10 echo T2- and 2) a diffusion weighted imaging (DWI) sequence in which each sequence collected 20 coronal slices (1 mm thickness and

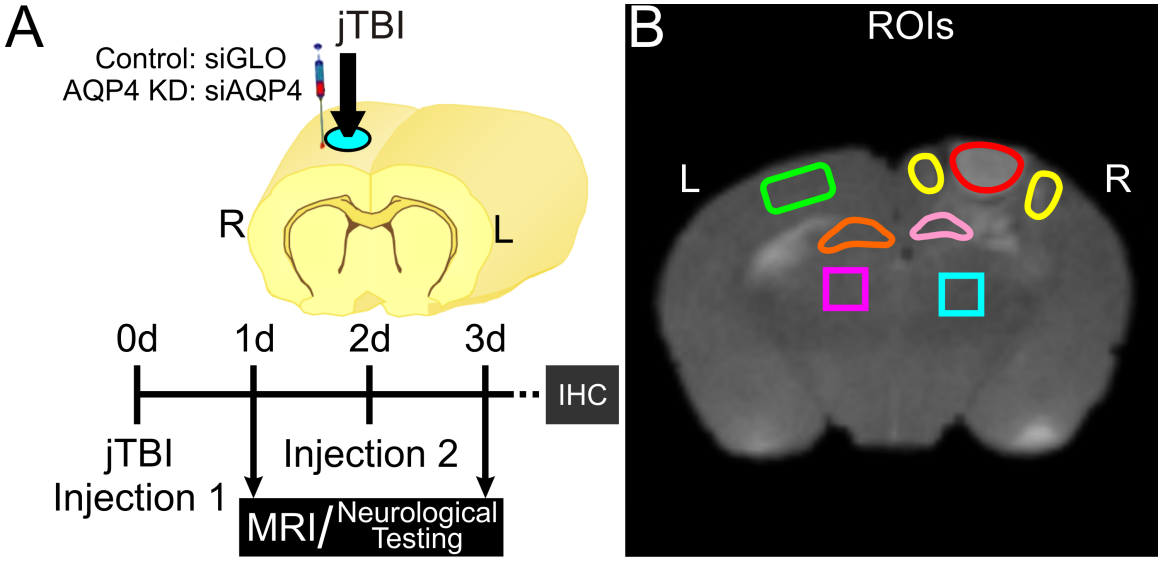

Figure 4.1: Experimental Design and Regions of Interest

A. Juvenile traumatic brain injury (jTBI) was induced in the right (R) parietal cortex of P17 rat pups. siRNA against aquaporin-4 (siAQP4) or non-targeted siRNA (siGLO) was injected lateral to the injury at 1 mm below the cortical surface (4 µl at 0.4 µl/min) immediately after injury and at 2 days post injury. Neurological testing was completed before each MRI scan at 1 and 3 days. Pups were then perfused for immunohistochemical (IHC) analysis after the last MRI scan at 3 days. B. Regions of interest (ROIs) were delineated on T2-weighted images (T2WI) and included the lesion (red), perilesion (yellow), contralateral cortex (green); and ipsi- and contralateral striatum (blue and purple) and hippocampus (pink and orange). Abbreviations: L = left hemisphere, KD = knockdown

interleaved by 1 mm). The 11.7T T2 sequence had the following parameters: TR/TE = 2357.9 / 10.2 ms, matrix = 128 x 128, field of view (FOV) = 2 cm, and 2 averages. The DWI sequence had the following parameters: TR/TE = 1096.5 / 50 ms, two b-values (116.960, 1044.422 s/mm^2), matrix = 128 x 128, FOV = 2 cm, and 2 averages. Total imaging time was 40 mins.

Region of Interest (ROI) and Volumetric Analysis. T2 relaxation rates were determined for each pixel and T2 maps were generated. Apparent diffusion coefficient (ADC) maps were calculated using a linear two-point fit. Region of interests (ROIs) were delineated on T2 images using Cheshire (PAREXEL International Corp., Waltham, MA) and included lesion, perilesion, contralateral cortex; and ipsi- and contralateral striatum and hippocampus (Fig. 4.1B). These ROIs were then overlaid onto the corresponding T2 and ADC maps. The mean, standard deviation, and area for each ROI were extracted.

Volumetric MR image analysis methods used are similar to that in our earlier studies (Ashwal et al., 2006). Using Amira software (Mercury Computer Systems, San Diego, CA), T2 images were analyzed using regions of hyperintensity to delineate the spatial development of the lesion volume. Analysis included lesion volume and ipsi- and contralateral hemispheric brain volumes. The lesion volume divided by the sum of both hemisphere volumes was used to obtain percent lesion to correct for individual brain size differences.

Neurological Testing*.* Neurological testing was measured at 1 and 3 days after CCI using beam balance to evaluate proprioception and balance, foot-

fault to evaluate sensorimotor response and proprioception, and rotarod to evaluate sensorimotor coordination. All testing was carried out within a 3-hour morning time block (6 – 9AM).

Beam Balance: The beam balance task was elevated 62 cm using a Plexiglas beam 60 cm long and 0.5 cm wide. At the center, pups were placed perpendicular to the beam and allowed to walk unrestricted in either direction. The duration spent on the beam without falling and distance traveled was recorded. The average of two trials per day, each trail not exceeding 60 sec, was used for statistical analysis.

Foot-fault: Rat pups were given 60 sec to explore a 50 cm by 155 cm platform (ClosetMaid, Ocala, FL) with parallel wires bars 1.5 cm apart. The apparatus was elevated 100 cm and the number of foot faults were recorded. A foot fault was defined as the misplacement of a fore- or hindlimb, such that the paw fell completely through the bars. The average of two trials per day was used for statistical analysis.

Rotarod: The rotarod (SD Instruments, San Diego, CA) consists of a rotating horizontal cylinder (7 cm diameter) divided into 10.5 cm wide lanes. Rat pups must continuously walk forward to avoid falling. The trial ended at 60 sec or when the pup fell off the cylinder; latency to fall was recorded. Rats were tested at two speeds, 10 and 20 RPM. The average of two trials per speed per day was used for statistical analysis.

Brain histology preparation. After the final imaging time point at 3 days, pups were deeply anesthetized (ketamine-xylazine) and transcardially perfused with 4% paraformaldehyde (PFA). After incubating in PFA for 24 hours, dissected brains were rinsed in phosphate buffered saline (PBS) solution, placed in 30% sucrose for 48 hours and stored at -20°C prior to cutting. The frozen brains were cut in coronal sections at -22°C on a cryostat (Leica, Richmond, IL) at 20 μm thickness.

Immunohistochemistry and image analysis. For immunofluorescence and infrared (IR) analysis, methods previously described were followed (Badaut et al., 2011a).

IgG staining for blood brain barrier (BBB) evaluation: Sections were washed with PBS for 20 minutes, blocked with 1% BSA in PBS, then incubated for 2 hours at room temperature with IR Dye 800 conjugated affinity purified goat-anti-rat immunoglobulin G (IgG, 1:500, Rockalnd, Gilbertsville, PA) in PBS containing 0.1% Triton X-100 and 1% bovine serum albumin. After washing, sections were scanned on an IR scanner (Odyssey) to quantify fluorescence in ROIs as previously described (Badaut et al., 2011a).

AQP4/ GFAP/ NeuN Immunohistochemistry: Rabbit polyclonal antibodies for AQP4 (Alpha Diagnostic, Owings Mill, MD), chicken polyclonal antibodies for glial fibrillary acidic protein (GFAP, Millipore, Billerica, MA), mouse monoclonal antibodies for endothelial barrier antigen (EBA, Covance, Princeton, NJ), and mouse monoclonal antibodies for neuronal nuclei (NeuN, Abcam, Cambridge,

MA) were used for immunohistochemistry. Sections were washed with PBS, blocked with 1% BSA in PBS, incubated with the respective primary antibodies overnight, then incubated with affinity purified secondaries conjugated to the desired wavelength to either be scanned on an IR scanner or to be observed under a confocal microscope (Olympus, Center Valley, PA). AQP4 and GFAP were quantified similar to IgG extravasation staining. EBA and NeuN staining was quantified with Mercator software (Explora-Nova, La Rochelle, France) where the area of EBA staining was measured and NeuN positive cells were counted. Negative control staining where the primary antibody or secondary antibody was omitted showed no detectable labelling.

Statistics. Using SigmaPlot (Systat Software Inc., San Jose, CA), data from foot-fault, beam balance, and rotarod tests were analyzed by two-way repeated measures analysis of variance (ANOVA) with a post hoc Bonferroni test. The Student's t-test was used for all ROI and volumetric analysis. One-way ANOVA was used for immunohistochemistry analysis. An α-level of 0.05 was used for all statistical significance tests. All data are expressed as the mean ± SEM.

Results

Reduced AQP4 Expression After siAQP4 Treatment. siAQP4 treatment resulted in decreased intensity of AQP4 staining around the lesion and was quantified using IR immunostaining (Fig. 4.2). We observed a 27% decrease in

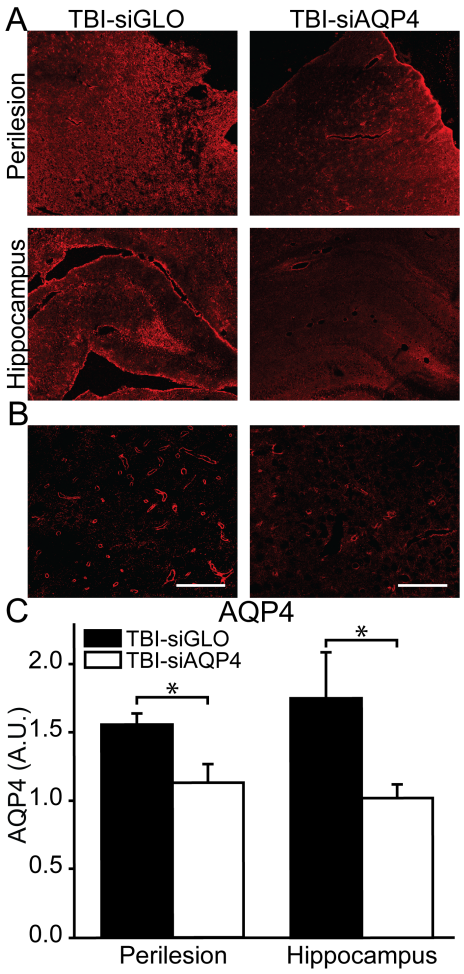

Figure 4.2: siAQP4 Treatment Decreases AQP4 Compared to siGLO after jTBI.

A. Representative images for AQP4 immunostaining in the perilesional cortex and hippocampus of TBI-siGLO and TBI-siAQP4 treated rat pups at low magnification. AQP4 staining was decreased in the TBI-siAQP4 compared to the TBI-siGLO group 3 days after injury. Similarly, significant decreases in AQP4 staining in the ipsilateral hippocampus of the TBI-siAQP4 group compared to TBI-siGLO. B. At higher magnification in the perilesional cortex, AQP4 staining is predominantly on astrocytic endfeet in contact with blood vessels in TBI-siGLO and TBI-siAQP4 rat pups, with decreased AQP4 staining in the TBI-siAQP4 group. This suggests that siAQP4 treatment after jTBI prevents the increase of AQP4 expression on the astrocyte endfeet. C. AQP4 immunostaining was quantified and confirmed a significant decrease in AQP4 immunofluorescence in TBI-siAQP4 compared to TBI-siGLO treated pups in both the perilesional cortex and ipsilateral hippocampus (*$p < 0.05$). Scale bars = 100 μm (Images provided by A. Fukuda and J. Badaut)

AQP4 expression within the perilesional tissue around the cavity on the ipsilateral cortex and a 33% decrease in the ipsilateral hippocampus in the siAQP4 rat pups after injury (TBI-siAQP4) as compared to TBI-siGLO pups ($p < 0.05$) (Fig 4.2C). The magnitude of the decrease in AQP4 staining after siAQP4 injection is similar to our previously published observations in normal juvenile brain tissues (Badaut et al., 2011a).

siAQP4 treatment prevents edema formation. siAQP4 treatment after jTBI decreased T2 (edema) and ADC (water mobility) values compared to the siGLO-treated pups at 1 and 3 days (Fig. 4.3A-D). From 1 to 3 days, T2 values increased in the lesion/perilesion area of TBI-siGLO pups but not in TBI-siAQP4 pups (Fig. 4.3B). AQP4 silencing resulted in 22% and 15% decrease in T2 values respectively in the lesion and ipsilateral hippocampus compared to TBI-siGLO rat pups at 3 days (Fig. 4.3B). ADC values were decreased by 21% in the lesion at 1 day ($p <0.005$) and 24% in the ipsilateral hippocampus at 3 days ($p < 0.001$) in TBI-siAQP4 compared to TBI-siGLO rats (Fig. 4.3D). All together, these data suggest less edema formation (T2) and improved tissue characteristics (ADC) in the tissues around the site of the impact in siAQP4-treated rats.

Lesion volume was also determined from T2 images where no differences were found between groups at 1 (2.7% ± 0.3 TBI-siGLO versus 2.7% ± 0.4 TBI-siAQP4) and 3 days (2.8% ± 0.4 TBI-siGLO versus 2.2% ± 0.5 TBI-siAQP4) (Fig. 4.3E). Interestingly, 86% of TBI-siAQP4 rats showed a decrease in lesion volumes between 1 and 3 days versus 56% of TBI-siGLO rats (Fig. 4.3F). These

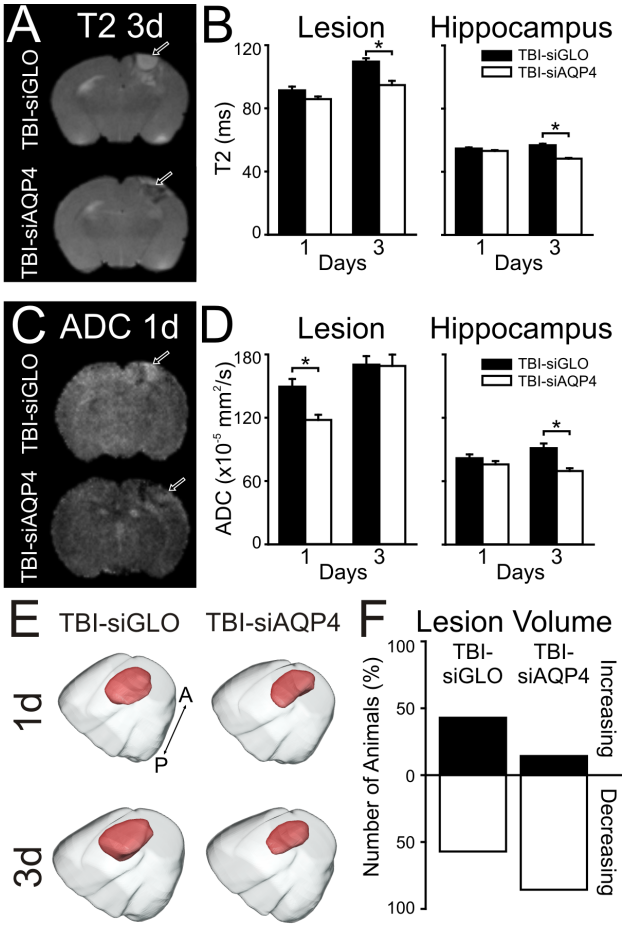

Figure 4.3: Quantitative Neuroimaging Reveals siAQP4 Treatment Decreases Edema.

A. Representative T2 images at 3 days in TBI-siGLO and TBI-siAQP4 treated rats show decreased edema at the lesion site (arrows) following siAQP4 treatment. B. TBI-siAQP4 pups had significantly decreased edema compared to siGLO pups within the lesion at 3 days (*p < 0.001). There was also a significant decrease in edema after siAQP4 treatment at 3 days within the hippocampus, ventral to the injury (*p < 0.02). C. Representative apparent diffusion coefficient (ADC) images show decreased water mobility in TBI-siAQP4 pups compared to siGLO treatment at 1 day it the lesion (arrows). D. Quantitative ADC revealed significantly decreased ADC values in TBI-siAQP4 pus in the lesion at 1 days compared to TBI-siGLO (*p < 0.005). TBI-siAQP4 pups also had significantly decreased ADC in the hippocampus at 3 days (*p < 0.001). E. Representative 3D brain reconstructions of lesion volumes in TBI-siGLO and TBI-siAQP4 rats at 1 and 3 days, where red denotes the lesion. F. In the TBI-siAQP4 group, there were a higher number of rats that had smaller lesion volumes at 3 days compared to 1 day. Abbreviations: A = anterior, P = posterior

data suggest a faster recovery or resolution of edema (lesion volume was calculated using T2 images) in TBI-siAQP4 compared to TBI-siGLO pups.

Reduced BBB Disruption in siAQP4-treated Rat Pups. BBB integrity after jTBI with siAQP4 or siGLO treatments was assessed with both IgG extravasation (Fig. 4.4A) and EBA staining (Fig. 4.4B). IgG extravasation staining intensity was decreased by 30% around the site of the injury in the TBI-siAQP4 group ($p < 0.05$) (Fig. 4.4C). In support to this result, a 31% increase in the area of EBA staining in TBI-siAQP4 compared to TBI-siGLO rat pups was observed (Fig 4.4D). The increased IgG staining signifies a more permeable blood brain barrier while the increased EBA staining points to increased intact blood vessels in siAQP4-treated rats after jTBI. siAQP4 treatment mitigated BBB disruption with more intact blood vessels by increased EBA staining and decreased IgG extravasation staining after jTBI.

Reduced Astrogliosis and Increased Neurons in siAQP4-treated Rat Pups. Astrogliosis was assessed with GFAP immunolabelling (Fig 4.5A, C). GFAP staining intensity was decreased by 39% around the tissue cavity and by 26% decrease in the ipsilateral hippocampus of TBI-siAQP4 rat pups as compared to TBI-siGLO ($p < 0.05$) (Fig 4.5C). These data showed that siAQP4 treatment results in a decrease in astrogliosis after jTBI.

Previous reports have described a decrease in NeuN positive cells in the perilesion after jTBI (Gobbel et al., 2007, Ajao et al., 2012). TBI-siGLO pups had 62% NeuN positive cells compared to TBI-siAQP4 pups in the perilesional cortex

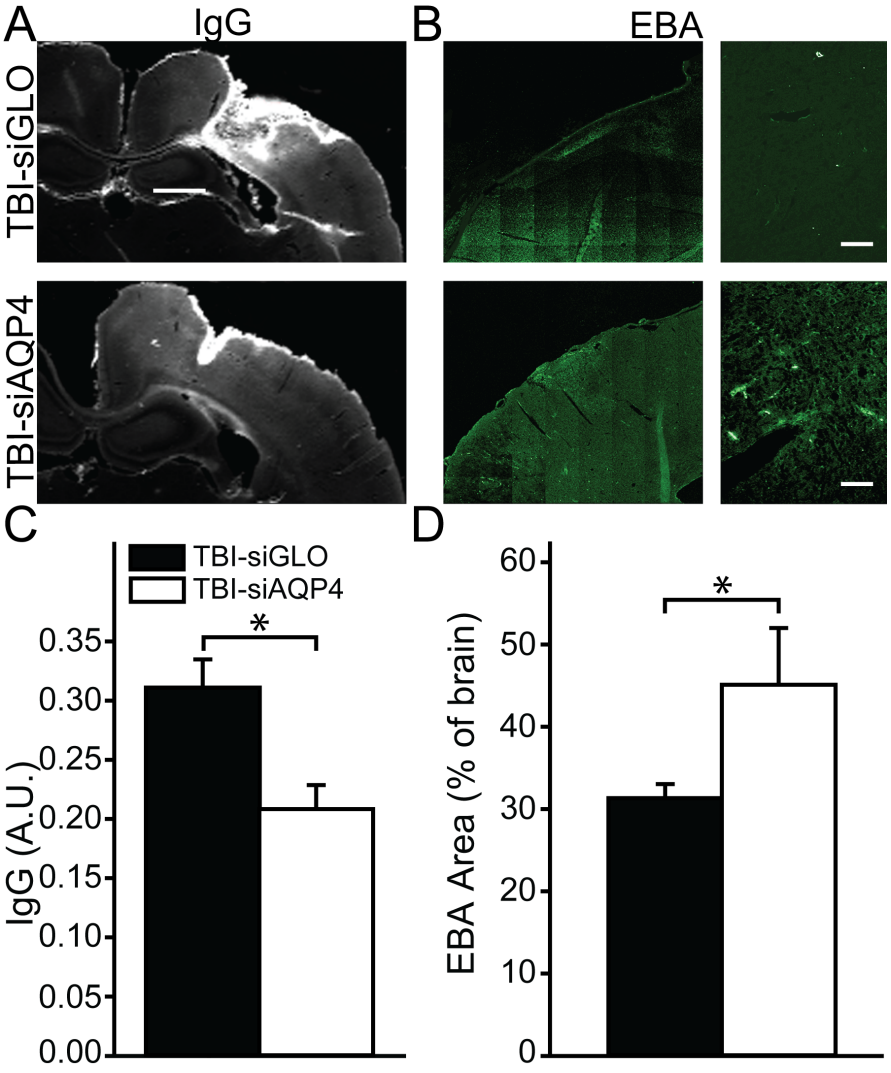

Figure 4.4: siAQP4 Prevents Blood-Brain Barrier (BBB) Disruption.

A. Representative images of immunoglobulin G (IgG) extravasation in TBI-siGLO and TBI-siAQP4 pups. B. Endothelial barrier antigen (EBA) staining is a marker of intact endothelial cells in rats and are shown in low (left panel) and high magnification (right panel). TBI-siGLO treated pups show blood vessels devoid of EBA staining. In contrast, TBI-siAQP4 staining had more EBA positive staining at higher magnification (right). C. TBI-siAQP4 rats had significantly less IgG extravasation adjacent to the lesion site compared to TBI-siGLO treated pups (*$p < 0.05$) suggesting that siAQP4 treatment mitigates blood-brain barrier (BBB) disruption. D. Quantification of EBA staining showed increased EBA positive staining in TBI-siAQP4 rats, suggesting fewer damaged blood vessels. Abbreviations: A.U. = arbitrary units. Scale bars = 100μm (Images provided by A. Fukuda and J. Badaut).

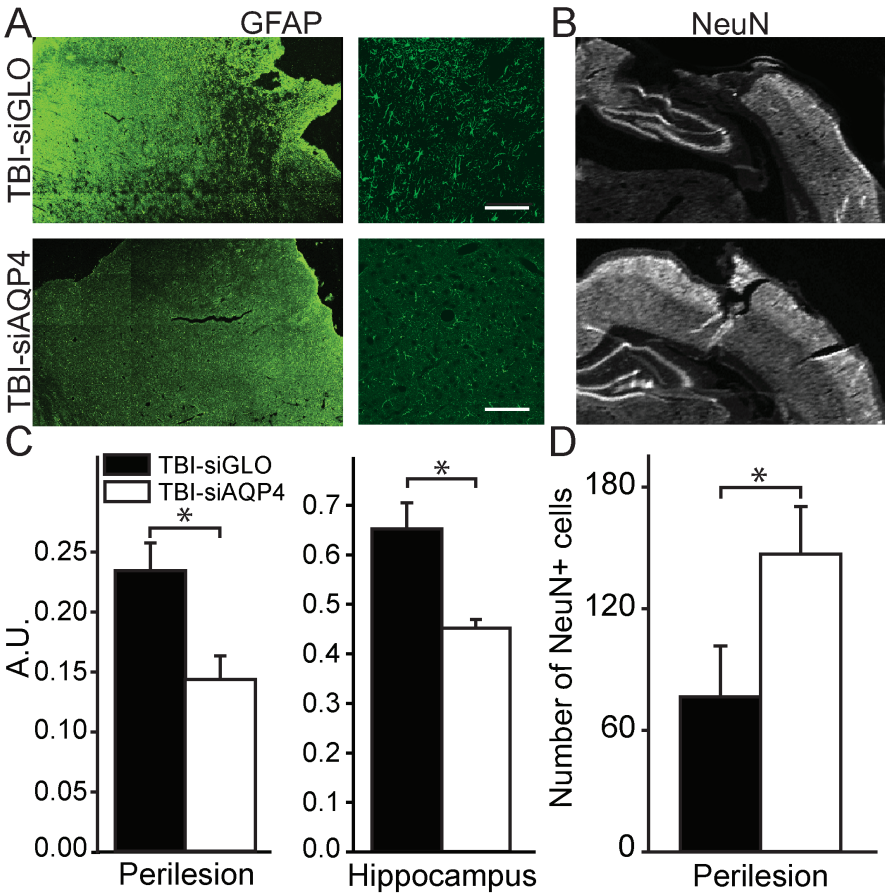

Figure 4.5: Reduced Astrogliosis after siAQP4 Treatment.

A. Representative images for glial fibrillary acidic protein (GFAP) staining in the perilesional cortex at low (left) and high magnification (right) in TBI-siGLO and TBI-siAQP4 rats 3 days after injury. GFAP staining in the region bordering the cavity (perilesion) was decreased in the TBI-siAPQ4 treated rats compared to the TBI-siGLO. At higher magnification, GFAP staining shows more GFAP positive cells with swollen cell bodies and processes in the TBI-siGLO group compared to TBI-siAQP4 in the perilesional cortex. B. Representative images of neuronal nuclei (NeuN) staining at 3 days. TBI-siAQP4 pups showed more staining compared to TBI-siGLO pups. C. The infrared intensity of GFAP staining was quantified and showed a significant decrease of GFAP staining in TBI-siAQP4 pups compared to TBI-siGLO in the perilesion and ipsilateral hippocampus (*$p < 0.05$). The significant decrease of GFAP in the siAQP4 treated rats suggests that siAQP4 treatment mitigates astrogliosis and the swelling of the astrocytes after jTBI. D. Neuronal cell counts revealed more NeuN positive cells in the perilesion of TBI-siAQP4 rats, suggesting improved neuronal survival after siAQP4 treatment (*$p < 0.05$). Scale bars = 100μm (Images provided by A. Fukuda and J. Badaut)

adjacent to the cavity and only 56% positive cells of TBI-siAQP4 in the ipsilateral hippocampus at 3 days (Fig. 4.5B, D). This result shows that siAQP4 treatment prevents the neuronal cell death associated with less astrogliosis.

Improved sensorimotor and proprioception recovery with siAQP4 treatment after jTBI. Concomitant with the observed decrease in edema and histological improvements, motor functions are also improved in siAQP4-treated rats after jTBI. TBI-siAQP4 pups had 34% fewer foot faults than TBI-siGLO pups at 1 day and 46% fewer foot faults at 3 days ($p < 0.05$, Fig 4.6A). Similarly, TBI-siAQP4 rats were able to stay on a rotarod 40% longer than TBI-siGLO rats at 3 days (Fig 4.6B).

Discussion

We report here for the first time that siAQP4 treatment is an effective mechanism for reducing edema after jTBI. The injection of siAQP4 induced decreased AQP4 expression by 30% leading to significant decrements in edema formation, less BBB disruption, decreased astrogliosis, reduced neuronal cell death and resulted in improved neurological function (proprioception and sensorimotor coordination). The uniqueness of our approach in implementing siRNA targeting AQP4 to improve functional outcomes after jTBI strongly suggests a potential future for clinical development.

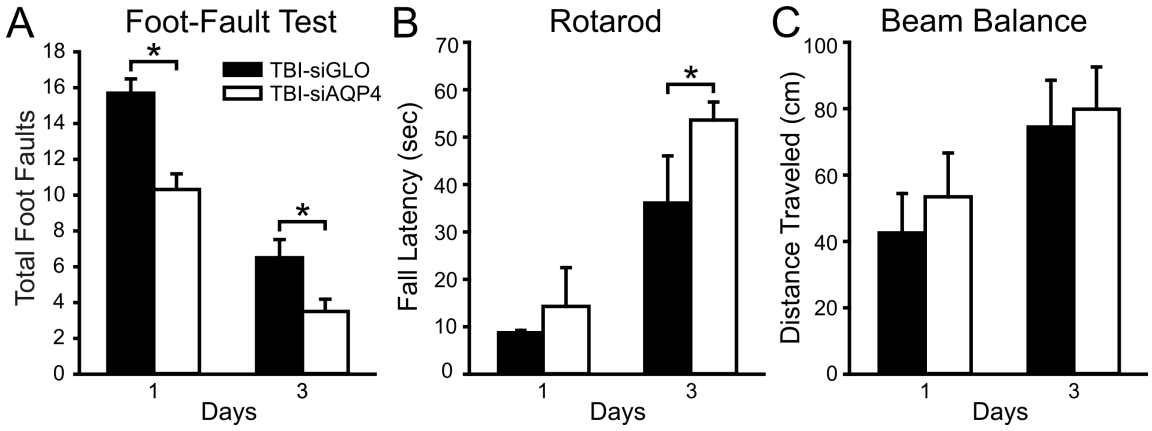

Figure 4.6: siAQP4 Treatment Improves Proprioception and Sensorimotor Recovery after jTBI.

A. siAQP4-treated pups had better functional outcomes as revealed by the foot-fault and rotarod tests. TBI-siAQP4 group had significantly fewer foot faults than TBI-siGLO at 1 (34%) and 3 days (46%) after jTBI (*$p < 0.05$). B. TBI-siAQP4 pups also performed better on the rotarod test at 3 days compared to TBI-siGLO pups by staying on for a significantly longer time before falling (*$p < 0.05$). C. Beam balance did not reveal any deficits in balance at any time points.

MRI (T2, ADC) was used to temporally monitor edema formation and lesion volume as is done in the clinic after brain injury (Obenaus and Ashwal, 2008, Chastain et al., 2009, Badaut et al., 2011b). Lesion volumes did not show any differences between groups. This is in accordance with the absence of differences in lesion volume after TBI in adult AQP4$^{-/-}$ and wild type (WT) mice (Shi et al., 2012). However, there were more animals in the TBI-siAQP4 group that had an improvement in lesion volume between 1 and 3 days, suggesting a difference in the rate of resolution of the lesion and edema and/or less edema formation (Fig. 4.3). This dynamic is supported by our observation that T2 values in TBI-siAQP4 rats had a significant decrease compared to TBI-siGLO group at 3 days, suggesting less water accumulation within the lesion/perilesion and hippocampal tissues (Fig. 4.3). The beneficial effects of siAQP4 were also observed in the ADC measurement, which is most often interpreted as water mobility. The increase of ADC values in the injury site may correspond to cell death leading to an altered tissue matrix. Interestingly, this increase in ADC is decreased in the TBI-siAQP4 compared to TBI-siGLO treated rat pups in the lesion, suggesting that the siAQP4 mitigates cell death at the early time point but not at 3 days within the lesion (Fig 4.3). However, in adjacent tissues such as the hippocampus, the ADC values were also significantly decreased, suggesting that siAQP4 possibly prevents cell death even at 3 days in the hippocampus by limiting the expansion of the edema formation. This hypothesis was supported by the increased numbers of neurons in the TBI-siAQP4 treated pups at 3 days (Fig.

4.5D). However, decreased ADC could also be associated with a decrease in AQP4 expression at 3 days (Fig. 4.2) in accordance with our previous work (Badaut et al., 2011a). In fact, decreased AQP4 expression has been correlated with decreased ADC (Meng et al., 2004, Badaut et al., 2011a) and increased AQP4 expression has been correlated with increased ADC (Tourdias et al., 2009) in rats. This suggests that water diffusion is limited by the decrease of AQP4 in the TBI-siAQP4 treatment group (Fig. 4.2). All together, the MRI data demonstrate that the siAQP4 treatment prevents edema formation with decreased T2 and ADC values in the lesion and ipsilateral hippocampus. At 3 days, T2 values are significantly higher in the lesion suggesting an increase in water content in the tissue due to the ongoing vasogenic edema formation in the untreated animals, while the decrease in the TBI-siAQP4 rats suggest that siAQP4 prevents vasogenic edema formation. This hypothesis is supported by the evidence of less BBB disruption (decreased IgG extravasation and increased EBA staining) in TBI-siAQP4 compared to TBI-siGLO pups. In fact, the injection of siAQP4 after jTBI may prevent water entry into astrocytes and block subsequent swelling of these cells at 1 day as indicated by the lower values of ADC in TBI-siAQP4 pups compared to TBI-siGLO. Less osmotic stress on the astrocytes may prevent BBB disruption by maintenance of the physical and mechanical properties of the endothelial cells and also neurovascular unit (Fig. 4.4). Therefore, less BBB disruption is associated with less extent of astrogliosis, which has been correlated with the severity of brain injury (Myer et al., 2006).

The beneficial effects of siAQP4 treatment was also observed in the higher number of neurons (NeuN positive cells) in TBI-siAQP4 compared to TBI-siGLO treated rats.

Finally, these improvements led to improved neurological outcomes at 1 and 3 days in TBI-siAQP4 treated rats (Fig. 4.6). Our results are in accordance with studies using knockout animals showing that $AQP4^{-/-}$ had improved outcomes compared to WT mice in cerebral pathologies such as hyponatremia (Papadopoulos and Verkman, 2005), bacterial meningitis (Papadopoulos and Verkman, 2005), water intoxication (Manley et al., 2000), focal cerebral ischemia (Manley et al., 2000), spinal cord injury (Saadoun et al., 2008), and encephalomyelitis (Li et al., 2009). Thus, the importance of the development of an AQP4 inhibitor cannot be underestimated. However, as noted earlier, no specific, effective drug directly against AQP4 is now available (Badaut et al., 2011b) despite promising studies using agents such as bumetanide (Migliati et al., 2009), acetazolamide (verkmanHuber et al., 2007, Tanimura et al., 2009) and methazolamide (Huber et al., 2009, Tanimura et al., 2009). Our study provides a novel therapeutic strategy to successfully target AQP4, leading to better outcomes after injury during the acute edema period. Our findings are unique demonstrating the proof of concept that siAQP4 treatment given twice after injury, with 30% decrease of AQP4 expression, is enough to achieve beneficial functional outcomes on edema formation, and functional improvements during the time-course of edema development.

The next step would be to investigate the most efficient method of delivery to the brain without craniotomy. One potential administration route would be intranasal delivery, which can bypass the BBB without complicated operations on the patients (Thorne et al., 1995, Liu et al., 2001a, Liu et al., 2001b, Thorne et al., 2004, Thorne et al., 2008). In summary, our novel findings provide compelling evidence for the effectiveness of siAQP4 as a potential therapeutic agent for not only jTBI, but for other cerebrovascular diseases involving edema as well.

Chapter 4 References

Ajao DO, Pop V, Kamper JE, Adami A, Rudobeck E, Huang L, Vlkolinsky R, Hartman RE, Ashwal S, Obenaus A, Badaut J (2012) Traumatic brain injury in young rats leads to progressive behavioral deficits coincident with altered tissue properties in adulthood. J Neurotrauma 29:2060-2074.

Ashwal S, Tone B, Tian HR, Chong S, Obenaus A (2006) Serial magnetic resonance imaging in a rat pup filament stroke model. Exp Neurol 202:294-301.

Ashwal S, Tone B, Tian HR, Chong S, Obenaus A (2007) Comparison of two neonatal ischemic injury models using magnetic resonance imaging. Pediatr Res 61:9-14.

Badaut J, Ashwal S, Adami A, Tone B, Recker R, Spagnoli D, Ternon B, Obenaus A (2011a) Brain water mobility decreases after astrocytic aquaporin-4 inhibition using RNA interference. J Cereb Blood Flow Metab 31:819-831.

Badaut J, Ashwal S, Obenaus A (2011b) Aquaporins in cerebrovascular disease: a target for treatment of brain edema? Cerebrovasc Dis 31:521-531.

Brody DL, Mac Donald C, Kessens CC, Yuede C, Parsadanian M, Spinner M, Kim E, Schwetye KE, Holtzman DM, Bayly PV (2007) Electromagnetic controlled cortical impact device for precise, graded experimental traumatic brain injury. J Neurotrauma 24:657-673.

Chastain CA, Oyoyo UE, Zipperman M, Joo E, Ashwal S, Shutter LA, Tong KA (2009) Predicting outcomes of traumatic brain injury by imaging modality and injury distribution. J Neurotrauma 26:1183-1196.

Fukuda AM, Adami A, Pop V, Bellone JA, Coats JS, Hartman RE, Ashwal S, Obenaus A, Badaut J (2013) Posttraumatic reduction of edema with aquaporin-4 RNA interference improves acute and chronic functional recovery. J Cereb Blood Flow Metab, doi:10.1038/jcbfm.2013.118.

Gobbel GT, Bonfield C, Carson-Walter EB, Adelson PD (2007) Diffuse alterations in synaptic protein expression following focal traumatic brain injury in the immature rat. Childs Nerv Syst 23:1171-1179.

Gotschall CS, Papero PH, Snyder HM, Johnson DL, Sacco WJ, Eichelberger MR (1995) Comparison of three measures of injury severity in children with traumatic brain injury. J Neurotrauma 12:611-619.

Huber VJ, Tsujita M, Kwee IL, Nakada T (2009) Inhibition of aquaporin 4 by antiepileptic drugs. Bioorg Med Chem 17:418-424.

Huber VJ, Tsujita M, Yamazaki M, Sakimura K, Nakada T (2007) Identification of arylsulfonamides as Aquaporin 4 inhibitors. Bioorg Med Chem Lett 17:1270-1273.

Kochanek PM (2006) Pediatric traumatic brain injury: quo vadis? Dev Neurosci 28:244-255.

Kochanek PM, Clark RS, Ruppel RA, Adelson PD, Bell MJ, Whalen MJ, Robertson CL, Satchell MA, Seidberg NA, Marion DW, Jenkins LW (2000) Biochemical, cellular, and molecular mechanisms in the evolution of secondary damage after severe traumatic brain injury in infants and children: Lessons learned from the bedside. Pediatr Crit Care Med 1:4-19.

Levin HS, Wilde EA, Chu Z, Yallampalli R, Hanten GR, Li X, Chia J, Vasquez AC, Hunter JV (2008) Diffusion tensor imaging in relation to cognitive and functional outcome of traumatic brain injury in children. J Head Trauma Rehabil 23:197-208.

Li L, Zhang H, Verkman AS (2009) Greatly attenuated experimental autoimmune encephalomyelitis in aquaporin-4 knockout mice. BMC Neuroscience 10:94.

Liu XF, Fawcett JR, Thorne RG, DeFor TA, Frey WH, 2nd (2001a) Intranasal administration of insulin-like growth factor-I bypasses the blood-brain barrier and protects against focal cerebral ischemic damage. J Neurol Sci 187:91-97.

Liu XF, Fawcett JR, Thorne RG, Frey WH, 2nd (2001b) Non-invasive intranasal insulin-like growth factor-I reduces infarct volume and improves neurologic function in rats following middle cerebral artery occlusion. Neurosci Lett 308:91-94.

Manley GT, Fujimura M, Ma T, Noshita N, Filiz F, Bollen AW, Chan P, Verkman AS (2000) Aquaporin-4 deletion in mice reduces brain edema after acute water intoxication and ischemic stroke. Nat Med 6:159-163.

Margulies S, Hicks R (2009) Combination therapies for traumatic brain injury: prospective considerations. J Neurotrauma 26:925-939.

Meng S, Qiao M, Lin L, Del Bigio MR, Tomanek B, Tuor UI (2004) Correspondence of AQP4 expression and hypoxic-ischaemic brain oedema monitored by magnetic resonance imaging in the immature and juvenile rat. The European Journal of Neuroscience 19:2261-2269.

Migliati E, Meurice N, DuBois P, Fang JS, Somasekharan S, Beckett E, Flynn G, Yool AJ (2009) Inhibition of aquaporin-1 and aquaporin-4 water permeability by a derivative of the loop diuretic bumetanide acting at an internal pore-occluding binding site. Mol Pharmacol 76:105-112.

Myer DJ, Gurkoff GG, Lee SM, Hovda DA, Sofroniew MV (2006) Essential protective roles of reactive astrocytes in traumatic brain injury. Brain 129:2761-2772.

Obenaus A, Ashwal S (2008) Magnetic resonance imaging in cerebral ischemia: focus on neonates. Neuropharmacology 55:271-280.

Obenaus A, Robbins M, Blanco G, Galloway NR, Snissarenko E, Gillard E, Lee S, Curras-Collazo M (2007) Multi-modal magnetic resonance imaging alterations in two rat models of mild neurotrauma. J Neurotrauma 24:1147-1160.

Papadopoulos MC, Manley GT, Krishna S, Verkman AS (2004) Aquaporin-4 facilitates reabsorption of excess fluid in vasogenic brain edema. FASEB J 18:1291-1293.

Papadopoulos MC, Verkman AS (2005) Aquaporin-4 gene disruption in mice reduces brain swelling and mortality in pneumococcal meningitis. J Biol Chem 280:13906-13912.

Recker R, Adami A, Tone B, Tian HR, Lalas S, Hartman RE, Obenaus A, Ashwal S (2009) Rodent neonatal bilateral carotid artery occlusion with hypoxia mimics human hypoxic-ischemic injury. J Cereb Blood Flow Metab 29:1305-1316.

Saadoun S, Bell BA, Verkman AS, Papadopoulos MC (2008) Greatly improved neurological outcome after spinal cord compression injury in AQP4-deficient mice. Brain 131:1087-1098.

Shi WZ, Zhao CZ, Zhao B, Zheng XL, Fang SH, Lu YB, Zhang WP, Chen Z, Wei EQ (2012) Aquaporin-4 deficiency attenuates acute lesions but aggravates delayed lesions and microgliosis after cryoinjury to mouse brain. Neuroscience Bulletin 28:61-68.

Simard M, Arcuino G, Takano T, Liu QS, Nedergaard M (2003) Signaling at the gliovascular interface. J Neurosci 23:9254-9262.

Tanimura Y, Hiroaki Y, Fujiyoshi Y (2009) Acetazolamide reversibly inhibits water conduction by aquaporin-4. J Struct Biol 166:16-21.

Thorne RG, Emory CR, Ala TA, Frey WH, 2nd (1995) Quantitative analysis of the olfactory pathway for drug delivery to the brain. Brain Res 692:278-282.

Thorne RG, Hanson LR, Ross TM, Tung D, Frey WH, 2nd (2008) Delivery of interferon-beta to the monkey nervous system following intranasal administration. Neuroscience 152:785-797.

Thorne RG, Pronk GJ, Padmanabhan V, Frey WH, 2nd (2004) Delivery of insulin-like growth factor-I to the rat brain and spinal cord along olfactory and trigeminal pathways following intranasal administration. Neuroscience 127:481-496.

Tong W, Igarashi T, Ferriero DM, Noble LJ (2002) Traumatic brain injury in the immature mouse brain: characterization of regional vulnerability. Exp Neurol 176:105-116.

Tourdias T, Dragonu I, Fushimi Y, Deloire MS, Boiziau C, Brochet B, Moonen C, Petry KG, Dousset V (2009) Aquaporin 4 correlates with apparent diffusion coefficient and hydrocephalus severity in the rat brain: a combined MRI-histological study. Neuroimage 47:659-666.

Verkman AS (2008) Mammalian aquaporins: diverse physiological roles and potential clinical significance. Expert Reviews in Molecular Medicine 10:e13.

Chapter 5

General Discussion

An extraordinary amount of insight has been gained about the workings of the nervous system after injury since the 18th century, when it was first suggested that intracranial pressure – and not skull damage – may be the cause of the sequelae after traumatic brain injury (TBI). The advancement of technologies that improved treatment and diagnosis, such as the development of imaging tools including computed tomography (CT) and magnetic resonance imaging (MRI), greatly increased during the 20th century. In the 1970s, increased awareness of TBI as a public health issue and the separation of brain injury into primary and secondary injury helped in the progression of brain trauma research. In order to test a therapeutic agent, we first characterized an established reproducible model of juvenile traumatic brain injury. We focused our study on two hallmarks of TBI – edema formation and extravascular blood deposition. Our study was novel in that we used noninvasive imaging to categorize animals into injury severity groups based on depression during CCI, serially tracked the changes in edema and blood in the lesion, and finally confirmed these changes with histology, which quantitatively measured cell death and identified the location of the hemorrhage.

After evaluation of different injury severities with MRI, we selected animals with moderate jTBI (1.5 mm depression). This group was selected as edema formation was still detectable after 3 days and the focal lesion was limited to one brain region, making it easy to create a standardized protocol for injection of siRNA therapy into the injured region. After the selection of CCI depth to produce moderate injury, we strived to demonstrate that small interfering RNA against AQP4 (siAQP4) could knock down protein expression *in vivo* without changing other tissue dynamics. We showed that siAQP4 injection into uninjured animals was able to reduce AQP4 protein expression by 27%, which lead to a 50% decrease in ADC values in brain regions both contralateral and ipsilateral to the injection site.

Using two different MRI modalities (T2 and DWI), we supported the therapeutic feasibility of using siAQP4 as a transient treatment for preventing edema formation after TBI. The reduction in edema led to improved neurological outcomes, which has not been shown before in the developing rodent brain. Further, we provided evidence that this effect can be monitored using MRI to noninvasively track lesion progression after injury. This convergence of evidence suggests that AQP4 is an important factor in the progression of early vasogenic edema and, thus worsening neurological outcomes, after brain injury. Interestingly, we did not see a change in the lesion volumes between jTBI pups treated with siAQP4 and siGLO. These findings suggest that, while AQP4 may play a role in the TBI injury process, it is not the sole mediator. The treatment of

TBI and vasogenic edema may require several drug targets. Future studies are needed to determine an ideal protocol for siRNA administration with variables including: 1) location of injection in relation to the lesion, 2) latency to intervention, 3) efficacy of multiple injections, and 4) efficacy of injection into other brain regions. The next steps for future studies will require higher order animals that more accurately mimic human functional anatomy to fully address the therapeutic potential of siAQP4. Nonetheless, the lack of specific therapeutic drugs targeting edema formation suggests that siAQP4 may play a valuable clinical role based on our early results.